

The automation of SMEFT-Assisted Constraints on UV-Complete Models

Jaco ter Hoeve,^{a,b} Giacomo Magni,^{a,b} Juan Rojo,^{a,b} Alejo N. Rossia,^c and Eleni Vryonidou^c

^a*Nikhef Theory Group, Science Park 105, 1098 XG Amsterdam, The Netherlands*

^b*Physics and Astronomy, Vrije Universiteit Amsterdam, NL-1081 HV Amsterdam, The Netherlands*

^c*Department of Physics and Astronomy, University of Manchester, Oxford Road, Manchester M13 9PL, United Kingdom*

E-mail: j.j.ter.hoeve@vu.nl, gmagni@nikhef.nl, j.rojo@vu.nl,
alejo.rossia@manchester.ac.uk, eleni.vryonidou@manchester.ac.uk

ABSTRACT: The ongoing Effective Field Theory (EFT) program at the LHC and elsewhere is motivated by streamlining the connection between experimental data and UV-complete scenarios of heavy new physics beyond the Standard Model (BSM). This connection is provided by matching relations mapping the Wilson coefficients of the EFT to the couplings and masses of UV-complete models. Building upon recent work on the automation of tree-level and one-loop matching in the SMEFT, we present a novel strategy automating the constraint-setting procedure on the parameter space of general heavy UV-models matched to dimension-six SMEFT operators. A new Mathematica package, `MATCH2FIT`, interfaces `MATCHMAKEREFT`, which derives the matching relations for a given UV model, and `SMEFIT`, which provides bounds on the Wilson coefficients by comparing with data. By means of this pipeline and using both tree-level and one-loop matching, we derive bounds on a wide range of single- and multi-particle extensions of the SM from a global dataset composed by LHC and LEP measurements. Whenever possible, we benchmark our results with existing studies. Our framework realises one of the main objectives of the EFT program in particle physics: deploying the SMEFT to bypass the need of directly comparing the predictions of heavy UV models with experimental data.

KEYWORDS: SMEFT, Beyond the Standard Model, LHC Phenomenology, EFT Matching

Contents


1	Introduction	2
2	Tree-level and one-loop matching in the SMEFT	3
2.1	Tree-level matching	4
2.2	One-loop matching	6
2.3	UV invariants and SMEFT matching	7
3	Implementation in SMEFiT	8
4	Results	12
4.1	One-particle models matched at tree level	13
4.2	Multi-particle models matched at tree level	21
4.3	Single-particle models matched at one-loop	26
5	Summary and outlook	27
A	Baseline SMEFiT global analysis	29
B	The MATCH2FIT package	32
C	Origin of the logarithms in 1-loop matching formulas.	34
D	Additional details on UV models.	38

1 Introduction

One of the main motivations for the ongoing Standard Model Effective Field Theory (SMEFT) program in particle physics, see [1] for a recent review, is to streamline the connection between experimental data and UV-complete scenarios of new physics beyond the Standard Model (BSM) that contain new particles which are too heavy to be directly produced at available facilities. In this paradigm, rather than comparing the predictions of specific UV-complete models directly with data to derive information on its parameters (masses and couplings), UV-models are first matched to the SMEFT and subsequently the resulting Wilson coefficients are constrained by means of a global EFT analysis including a broad range of observables.

The main advantage of this approach is to bypass the need to recompute predictions for physical observables with different UV-complete models. The global SMEFT analysis essentially encapsulates, for a well-defined set of assumptions, the information provided by available experimental observables, while the matching relations determine how this information relates to the masses and couplings of the UV-complete model. This feature becomes specially relevant whenever new BSM models are introduced: one can then quantify to which extent their parameter space is constrained by current data from a pre-existing global SMEFT analysis, rather than having first to provide predictions for a large number of observables and then compare those with data.

In recent years, several groups [2–15] have systematically studied the matching between UV-complete models and the Wilson coefficients of the SMEFT, with various degrees of automation and in many cases accompanied by the release of the corresponding open-source codes. In order to realise the full potential of such EFT matching studies, it is however necessary to interface these results with global SMEFT analyses parameterizing the constraints provided by the experimental data. Such an interface must be constructed in a manner that benefits from the automation of EFT matching tools and that does not impose restrictions in the type of UV-models to be matched. In particular, it must admit non-linear matching relations with additional constraints such as parameter positivity. Several groups have reinterpreted global SMEFT fits in terms of matched UV models [16–18], but their focus is limited to pre-determined, relatively simple models with few parameters. No framework has been released to date that enables performing such fits with generic, user-specified, multi-particle UV-complete models.

Here we bridge this gap in the SMEFT literature by developing a framework automating the limit-setting procedure on the parameter space of generic UV-models which can be matched to dimension-six SMEFT operators. This is achieved by extending SMEFT [19–23] with the capabilities of working directly on the parameter space of UV-models, given arbitrary matching relations between UV couplings and EFT coefficients as an input. To this end, we have designed an interface to the MATCHMAKEREFT code [12] such that for any of the available UV-models it outputs a run card with the relevant Wilson coefficients entering the SMEFT analysis. This interface, consisting of the Mathematica package MATCH2FIT (available on [Github](#) ) , also provides a list of the UV variables (denoted as UV-invariants) that can be inferred from the data and corresponding to specific combinations of UV couplings and masses. The adopted procedure removes any limitations on the type of matching relations involved.

We exploit this new pipeline to derive bounds on a broad range of UV-complete scenarios both at linear and quadratic order in the SMEFT expansion from a global dataset composed by LHC and LEP measurements, using either tree-level or one-loop matching relations. We consider both relatively simple single-particle extensions of the SM as well as more complex multi-particle extensions, in particular with a benchmark model composed by two heavy vector-like fermions and one heavy vector boson. We study the stability of the fits results with respect to the order in the EFT expansion and the perturbative QCD accuracy for the EFT cross-sections. Whenever possible, we compare our results with existing SMEFT matching studies in the literature.

The framework presented in this work is made publicly available both in terms of the latest SMEFT release and with the independent MATCH2FIT interface, providing a valuable resource for the EFT community streamlining the connection between UV-models and EFT studies. Our work brings one step closer one of

the primary goals of the SMEFT program: constraining the parameters of general BSM Lagrangians using EFTs as a bridge between UV models and experimental data.

The structure of this paper is as follows. First, Sect. 2 discusses the general strategy adopted to automate the matching between UV-models and the corresponding SMEFT fits. Sect. 3 describes how the SMEFT framework is extended to enable constraint-setting directly in the parameter space of UV-complete models. The main results of this work are presented in Sect. 4, where we derive bounds on single- and multi-particle BSM models from a global dataset and compare our findings with existing results. We conclude and summarise possible future developments in Sect. 5.

Technical details of our work are provided in the appendices. App. A summarises the baseline SMEFT analysis used, in particular reporting on a recent update concerning the description of electroweak precision observables (EWPOs) from electron-positron colliders. App. B presents a concise description of the MATCH2FIT package. App. C discusses the origin of the logarithms arising in the one-loop matching formulae. Additional details on the single-particle model fits from Sect. 4 are provided in App. D.

2 Tree-level and one-loop matching in the SMEFT

The low-energy phenomenology of a quantum field theory can in many cases be described by an EFT with a reduced number of dynamical degrees of freedom. This feature presents clear advantages in terms of BSM searches, since a general-enough EFT could describe a plethora of different UV completions. The success of the Standard Model in describing the physics explored at the energy scales accessible by current experiments justifies the use of an EFT based upon it, which is known as the SMEFT [1, 24], to search for BSM physics in a model-independent manner. To ensure that the UV theory and the low-energy EFT predict the same observables in the energy range where the EFT is valid, the Wilson coefficients of the latter must be computed in terms of the parameters of the UV theory. This procedure is called matching.

Matching an EFT, such as the SMEFT, with the associated UV-complete model can be performed by means of two well-established techniques, as well as with another recently developed method based on on-shell amplitudes [15]. The first of these matching techniques is known as the functional method and is based on the manipulation of the path integral, the action, and the Lagrangian [2, 5, 7, 8, 11, 25]. It requires to specify the UV-complete Lagrangian, the heavy fields, and the matching scale, while the EFT Lagrangian is part of the result although not necessarily in the desired basis. The second technique is the diagrammatic method, based on equating off-shell Green's functions computed in both the EFT and the UV model, and therefore it requires the explicit form of both Lagrangians from the onset [3, 12]. Both methods provide the same final results and allow for both tree-level and one-loop matching computations. The automation of this matching procedure up to the one-loop level is mostly solved in the case of the diagrammatic technique [12], and is well advanced in the functional method case [4, 14].

Let us illustrate the core ideas underlying this procedure by reviewing the matching to the SMEFT at tree and one-loop level of a specific benchmark UV-complete model. This is taken to be the single-particle extension of the SM resulting from adding a new heavy scalar boson, ϕ . This scalar transforms under the SM gauge group in the same manner as the Higgs boson, i.e. $\phi \sim (1, 2)_{1/2}$, where we denote the irreducible representations under the SM gauge group as $(SU(3)_c, SU(2)_L)_{U(1)_Y}$. Following the notation of [3], the Lagrangian of this model reads

$$\begin{aligned} \mathcal{L}_{\text{UV}} = & \mathcal{L}_{\text{SM}} + |D_\mu \phi|^2 - m_\phi^2 \phi^\dagger \phi - \left((y_\phi^e)_{ij} \phi^\dagger \bar{e}_R^i \ell_L^j + (y_\phi^d)_{ij} \phi^\dagger \bar{d}_R^i q_L^j \right. \\ & \left. + (y_\phi^u)_{ij} \phi^\dagger i \sigma_2 \bar{q}_L^T i w_R^j + \lambda_\phi \phi^\dagger \varphi |\varphi|^2 + \text{h.c.} \right) - \text{scalar potential}, \end{aligned} \quad (2.1)$$

with \mathcal{L}_{SM} being the SM Lagrangian and φ the SM Higgs doublet. We do not write down explicitly the complete form of the scalar potential in Eq. (2.1), of which $\lambda_\phi \phi^\dagger \varphi |\varphi|^2$ is one of the components, since it has no further effect on the matching outcome as long as it leads to an expectation value satisfying $\langle \phi \rangle = 0$, such that $m_\phi^2 > 0$ corresponds to the pole mass.

Operator type	Generated operators
X^3	$\overline{\mathcal{O}}_W$
φ^6	$\overline{\mathcal{O}}_\varphi$
$\varphi^4 D^2$	$\overline{\mathcal{O}}_{\varphi\Box}, \overline{\mathcal{O}}_{\varphi D}$
$\psi^2 \varphi^3$	$\overline{\mathcal{O}}_{u\varphi}, \overline{\mathcal{O}}_{d\varphi}, \overline{\mathcal{O}}_{e\varphi}$
$X^2 \varphi^2$	-
$\psi^2 X \varphi$	$\overline{\mathcal{O}}_{dB}, \overline{\mathcal{O}}_{dG}, \overline{\mathcal{O}}_{dW}, \overline{\mathcal{O}}_{uB}, \overline{\mathcal{O}}_{uG}, \overline{\mathcal{O}}_{uW}, \mathcal{O}_{eB}, \mathcal{O}_{eW}$
$\psi^2 \varphi^2 D$	$\overline{\mathcal{O}}_{\varphi u}, \overline{\mathcal{O}}_{\varphi d}, \overline{\mathcal{O}}_{\varphi e}, \overline{\mathcal{O}}_{\varphi\ell}^{(1)}, \overline{\mathcal{O}}_{\varphi\ell}^{(3)}, \overline{\mathcal{O}}_{\varphi q}^{(1)}, \overline{\mathcal{O}}_{\varphi q}^{(3)}, \overline{\mathcal{O}}_{\varphi ud}$
ψ^4	$\overline{\mathcal{O}}_{qu}^{(1)}, \overline{\mathcal{O}}_{qu}^{(8)}, \overline{\mathcal{O}}_{le}, \overline{\mathcal{O}}_{lequ}^{(1)}, \overline{\mathcal{O}}_{qd}^{(1)}, \overline{\mathcal{O}}_{qd}^{(8)}, \overline{\mathcal{O}}_{quqd}^{(1)}, \mathcal{O}_{ledq},$ $\overline{\mathcal{O}}_{uu}, \overline{\mathcal{O}}_{dd}, \overline{\mathcal{O}}_{ll}, \overline{\mathcal{O}}_{ld}, \overline{\mathcal{O}}_{ee}, \overline{\mathcal{O}}_{ed}, \overline{\mathcal{O}}_{eu}, \overline{\mathcal{O}}_{lq}^{(1)}, \overline{\mathcal{O}}_{lq}^{(3)},$ $\overline{\mathcal{O}}_{lu}, \overline{\mathcal{O}}_{qe}, \overline{\mathcal{O}}_{qq}^{(1)}, \overline{\mathcal{O}}_{qq}^{(3)}, \overline{\mathcal{O}}_{quqd}^{(8)}, \overline{\mathcal{O}}_{ud}^{(1)}, \overline{\mathcal{O}}_{ud}^{(8)}, \mathcal{O}_{lequ}^{(3)}.$

Table 2.1: SMEFT dimension-6 operators in the Warsaw basis generated by the integration of the heavy doublet scalar ϕ from the Lagrangian defined in Eq. (2.1). The operators generated at tree level are highlighted in blue, while the operators that appear at one-loop level are in black. We assume that the non-vanishing couplings of this heavy particle with the SM are λ_ϕ and $(y_\phi^\psi)_{ij} = \delta_{i,3}\delta_{j,3}(y_\phi^\psi)_{33}$ for $\psi = u, d, e$. The operators with a bar over their name survive the further constraint of $(y_\phi^e)_{33} = (y_\phi^d)_{33} = 0$, required to fulfil the SMEFT flavour assumption at tree level. We take all the SM Yukawa couplings and masses to be zero, except those for the third-generation fermions.

This heavy doublet ϕ interacts with the SM fields via the Yukawa couplings $(y_\phi^{u,d,e})_{ij}$, the scalar coupling λ_ϕ , and the electroweak gauge couplings. In the following, we consider as ‘‘UV couplings’’ exclusively those couplings between UV and SM particles that are not gauge couplings. The model described by Eq. (2.1) corresponds to the two-Higgs doublet model (2HDM) in the decoupling limit [26, 27]. For simplicity, we assume that all the couplings between the SM and the heavy particle are real and satisfy $(y_\phi^\psi)_{ij} = \delta_{i,3}\delta_{j,3}(y_\phi^\psi)_{33}$ for $\psi = u, d, e$, and the only SM Yukawa couplings that we consider as non-vanishing are the ones of the third-generation fermions.

2.1 Tree-level matching

The matching of UV-complete models to dimension-6 SMEFT operators at tree level has been fully tackled in [3], which considers all possible UV-completions with particles of spin up to $s = 1$ generating non-trivial Wilson coefficients. These results can be reproduced with the automated codes MATCHINGTOOLS [28] and MATCHMAKEREFT [12] based on the diagrammatic approach. At tree level, the diagrammatic method requires computing the tree-level Feynman diagrams contributing to multi-point Green’s functions with only light external particles. Then, the covariant propagators Δ_i must be expanded to a given order in inverse powers of the heavy masses. The computation of the Feynman diagrams in the EFT can be performed in a user-defined operator basis.

The outcome of matching the model defined by the Lagrangian in Eq. (2.1) to the SMEFT at tree level is provided in [3]. Table 2.1 summarizes the dimension-6 operators in the Warsaw basis [29] generated by both tree-level (in blue) and one-loop (in black) matching. A representative subset of the resulting

tree-level matching expressions is given by

$$\begin{aligned} \frac{\left(c_{qd}^{(1)}\right)_{3333}}{\Lambda^2} &= -\frac{\left(y_\phi^d\right)_{33}^2}{6 m_\phi^2}, & \frac{\left(c_{qd}^{(8)}\right)_{3333}}{\Lambda^2} &= -\frac{\left(y_\phi^d\right)_{33}^2}{m_\phi^2}, & \frac{\left(c_{d\varphi}\right)_{33}}{\Lambda^2} &= \frac{\lambda_\phi \left(y_\phi^d\right)_{33}}{m_\phi^2}, & \frac{c_\varphi}{\Lambda^2} &= \frac{\lambda_\phi^2}{m_\phi^2}, \\ \frac{\left(c_{qu}^{(1)}\right)_{3333}}{\Lambda^2} &= -\frac{\left(y_\phi^u\right)_{33}^2}{6 m_\phi^2}, & \frac{\left(c_{qu}^{(8)}\right)_{3333}}{\Lambda^2} &= -\frac{\left(y_\phi^u\right)_{33}^2}{m_\phi^2}, & \frac{\left(c_{u\varphi}\right)_{33}}{\Lambda^2} &= -\frac{\lambda_\phi \left(y_\phi^u\right)_{33}}{m_\phi^2}, & \frac{\left(c_{\varphi q}\right)_{33}}{\Lambda^2} &= 0. \end{aligned} \quad (2.2)$$

Eq. (2.2) showcases the type of constraints on the EFT coefficients that tree-level matching can generate. First of all, the relations between UV couplings and Wilson coefficients will be in general non-linear. Second, some coefficients such as $\left(c_{\varphi q}^{(3)}\right)_{33}$ are set to zero by the matching relations. Third, other coefficients acquire a well-defined sign, such as $c_\varphi \left(\left(c_{qd}^{(1)}\right)_{3333}\right)$ which becomes positive-definite (negative-definite) after matching. Fourth, several EFT coefficients become related among them by means of both linear and non-linear relations such as

$$\left(c_{qu}^{(8)}\right)_{3333} = 6 \left(c_{qu}^{(1)}\right)_{3333}, \quad (2.3)$$

$$\frac{\left(c_{qd}^{(1)}\right)_{3333}}{\left(c_{qu}^{(1)}\right)_{3333}} = \left(\frac{\left(c_{d\varphi}\right)_{33}}{\left(c_{u\varphi}\right)_{33}}\right)^2. \quad (2.4)$$

These relations must be taken into account when performing the EFT fit to the experimental data, using the dedicated techniques discussed in Sect. 3 and App. A.

When considering multi-particle UV scenarios, rather than single-particle extensions such as the model defined by Eq. (2.1), non-vanishing EFT coefficients generally consist of the sum of several rational terms. For example, assume that one adds to the model of Eq. (2.1) a second heavy scalar with gauge charges $\Phi \sim (8, 2)_{1/2}$ and with mass m_Φ which couples to the SM fields by means of

$$\mathcal{L}_{UV} \supset -\left(y_\Phi^{qu}\right)_{ij} \Phi^{A\dagger} i\sigma_2 \bar{q}_{L,i}^T T^A u_{R,j} + \text{h.c.} . \quad (2.5)$$

Integrating out this additional heavy scalar field modifies two of the tree-level matching relations listed in Eq. (2.2) as follows

$$\frac{\left(c_{qu}^{(1)}\right)_{3333}}{\Lambda^2} = -\frac{\left(y_\phi^u\right)_{33}^2}{6 m_\phi^2} - \frac{2 \left(y_\Phi^{qu}\right)_{33}^2}{9 m_\Phi^2}, \quad \frac{\left(c_{qu}^{(8)}\right)_{3333}}{\Lambda^2} = -\frac{\left(y_\phi^u\right)_{33}^2}{m_\phi^2} + \frac{\left(y_\Phi^{qu}\right)_{33}^2}{6 m_\Phi^2}. \quad (2.6)$$

Hence, the simple linear relation Eq. (2.3) is not valid anymore, while Eq. (2.4) now becomes

$$\frac{\left(c_{qd}^{(1)}\right)_{3333}}{\frac{1}{9} \left(c_{qu}^{(1)}\right)_{3333} + \frac{4}{27} \left(c_{qu}^{(8)}\right)_{3333}} = \left(\frac{\left(c_{d\varphi}\right)_{33}}{\left(c_{u\varphi}\right)_{33}}\right)^2, \quad (2.7)$$

which shows that multiplicative relations might involve non-trivial linear combinations of the Wilson coefficients. In this context, we observe that many of the conditions on the EFT coefficients imposed by assuming a certain UV completion are non-linear and hence the resulting posterior distributions inferred from the data will in general be non-Gaussian.

The tree-level matching results discussed up to now do not comply with the flavour symmetry adopted by the current SMEFIT analysis, namely $U(2)_q \times U(2)_u \times U(3)_d \times (U(1)_\ell \times U(1)_e)^3$. This would cause ambiguities at the moment of performing the fit, since for example SMEFIT assumes that the coefficient $\left(c_{qd}^{(1)}\right)_{33ii}$ has the same value for $i = 1, 2, 3$, while the matching result instead gives a non-vanishing

coefficient only for $i = 3$. In this specific case, the appropriate flavour symmetry used at the EFT fit level can be respected after tree-level matching by further imposing

$$(y_\phi^e)_{33} = (y_\phi^d)_{33} = 0, \quad (2.8)$$

and leaving λ_ϕ and $(y_\phi^u)_{33}$ as the only non-vanishing UV couplings, as we will assume in the rest of this work unless otherwise specified. Notice that this implies that the heavy new particle interacts only with the Higgs boson and the top quark, a common situation in well-motivated UV models. The operators that remain after this additional restriction is imposed are indicated with a bar in Table 2.1.

Once this flavour symmetry is imposed, one can map unambiguously the naming of the operators and EFT coefficients provided by the MATCHMAKEREFT output to the ones defined in SMEFIT. The non-vanishing coefficients after integrating out the heavy scalar ϕ at tree level are then

$$c_\varphi = c_\varphi, \quad c_{t\varphi} = (c_{u\varphi})_{33}, \quad c_{Qt}^{(1)} = (c_{qu}^{(1)})_{3333}, \quad c_{Qt}^{(8)} = (c_{qu}^{(8)})_{3333}, \quad (2.9)$$

where in the l.h.s. of the equalities we use the SMEFIT convention and on the r.h.s the Warsaw convention adopted in the matching output [3, 12].

2.2 One-loop matching

Extending the diagrammatic matching technique to the one-loop case is conceptually straightforward, and requires the computation of one-loop diagrams in the UV model with off-shell external light particles and at least one heavy-particle propagator inside the loop. From the EFT side, diagrammatic matching at one-loop involves the calculation of the diagrams with the so-called Green's basis, which includes also those operators that are redundant by equations of motion (EoMs). The dimension-6 and dimension-8 Green's bases in the SMEFT have been computed in [6, 30, 31]. Further technicalities such as evanescent operators acquire special relevance at this order [13]. The automation of one-loop matching with the diagrammatic technique is provided by MATCHMAKEREFT [12] for any renormalisable UV model with heavy scalar bosons and spin-1/2 fermions. The equivalent automation applicable to models containing heavy spin-1 bosons is work in progress.

In this work we use MATCHMAKEREFT (v1.1.3) to evaluate the one-loop matching of a selected UV model. When applied to the Lagrangian of Eq. (2.1) with the SMEFIT flavour assumptions, this procedure generates additional non-vanishing operators in comparison to those arising at tree level, as indicated in Table 2.1, where we also show operators generated in the more general case of

$$(y_\phi^\psi)_{ij} = \delta_{i,3}\delta_{j,3} (y_\phi^\psi)_{33}, \quad \psi = e, u, d. \quad (2.10)$$

Notice that setting $(y_\phi^e)_{33} = (y_\phi^d)_{33} = 0$ has a smaller impact on the number of loop-generated operators than for the tree-level case. The reason is that, in many cases, the operators are still generated via SM-gauge couplings so the EFT coefficients take the generic form $c \sim g_{\text{SM}}^4/16\pi^2$. These contributions are typically flavour-universal and if they break the desired flavour symmetry, the breaking is suppressed by the SM gauge couplings and/or the loop factor. For this reason, in this work we only enforce the SMEFIT flavour symmetry for tree-level matching.

An example of the results of one-loop matching corrections to the EFT coefficients is provided for $c_{Qt}^{(8)}$, for which the tree-level matching relation in Eq. (2.2) is now extended as follows

$$\begin{aligned} \frac{c_{Qt}^{(8)}}{\Lambda^2} &= -\frac{(y_\phi^u)_{33}^2}{m_\phi^2} - \left[\frac{25g_1^2}{1152\pi^2} + \frac{3g_2^2}{128\pi^2} - \frac{3(y_t^{\text{SM}})^2}{16\pi^2} + \frac{g_3^2}{16\pi^2} \left(1 - \log \left(\frac{m_\phi^2}{\mu^2} \right) \right) \right] \frac{(y_\phi^u)_{33}^2}{m_\phi^2} \\ &+ \frac{3}{64\pi^2} \left[1 - 2 \log \left(\frac{m_\phi^2}{\mu^2} \right) \right] \frac{(y_\phi^u)_{33}^4}{m_\phi^2}, \end{aligned} \quad (2.11)$$

with μ being the matching scale, g_i the SM gauge coupling constants, and y_t^{SM} the top Yukawa coupling in the SM. To estimate of the numerical impact of loop corrections to matching in the specific case of Eq. (2.11), one can substitute the corresponding values of the SM couplings. One finds that the term proportional to $\left(y_\phi^u\right)_{33}^2$ receives a correction at the few-percent level from one-loop matching effects.

The logarithms in the matching scale μ appearing in Eq. (2.11) are generated by the running of the couplings and Wilson coefficients between the heavy particle mass m_ϕ and μ , as further discussed in App. C. Since here we neglect RGE effects [32], we simplify the matching expressions by choosing the scale μ to be equal to the mass of the integrated-out UV heavy field such that the logarithms vanish.

As compared to the tree-level matching relations, common features of the one-loop contributions are the appearance of terms proportional to the UV couplings at the fourth order and the presence of the SM gauge couplings. Here we assume that the latter have fixed numerical values determined by other measurements i.e. the PDG averages [33]. This implies that at the fit level some of the EFT coefficients are specified entirely by the mass of the UV heavy particle, such as for the dimension-six triple SU(2) field strength tensor operator for the considered model

$$\frac{c_{WWW}}{\Lambda^2} = \frac{g_2^3}{5760\pi^2 m_\phi^2}. \quad (2.12)$$

While one may expect that one-loop matching relations such as Eq. (2.12), which depend only on the gauge couplings of the heavy particle and its mass, provide useful sensitivity to the heavy mass m_ϕ , we have verified that this is in practice very weak and hence not competitive.

It is also possible to find EFT coefficients that are matched to the sum of a piece depending only on SM couplings and the UV mass and a piece proportional to the UV couplings, e.g.,

$$\frac{c_{\varphi Q}^{(3)}}{\Lambda^2} = -\frac{g_2^4}{3840\pi^2 m_\phi^2} - \frac{(y_t^{\text{SM}})^2 \left(y_\phi^u\right)_{33}^2}{192\pi^2 m_\phi^2} + \frac{g_2^2 \left(y_\phi^u\right)_{33}^2}{1152\pi^2 m_\phi^2}. \quad (2.13)$$

This kind of relations could in principle favour non-vanishing UV couplings even when the EFT coefficients are very tightly constrained, provided that the gauge-coupling term is of similar size to the other terms in the matching relation.

As for tree-level matching, exemplified by Eqns. (2.3) and (2.4), at the one-loop level one can also automatically evaluate linear relations among the Wilson coefficients, though the analogous result for non-linear relations is more challenging. Nevertheless, as discussed in Sect. 3, in this work we carry out the fit directly at the level of UV couplings and hence the constraints between different coefficients are provided implicitly by the matching relations, rather than directly as explicit restrictions in a fit of EFT coefficients.

2.3 UV invariants and SMEFT matching

The inverse problem to matching lies at the heart of the interpretation of the SMEFT global fit results in terms of UV couplings and masses. This inverse problem is known to be plagued by degeneracies since many UV completions could yield the same EFT coefficients up to a fixed mass dimension [34]. Matching relations define a mapping f from U , the parameter space spanned by the UV couplings \mathbf{g} , to W , the space spanned by the Wilson coefficients \mathbf{c} ,

$$f : U \rightarrow W. \quad (2.14)$$

The previous discussion indicates that the matching relation f associated to UV-models such as the one defined by Eq. (2.1) is in general non-injective and hence non-invertible. Therefore, even choosing a particular UV model does not lift completely these degeneracies. They might be partially or fully removed by either matching at higher loop orders or considering higher-dimensional operators. In particular, dimension-8 operators offer advantages to disentangle UV models [34], but their study is beyond the scope of this work.

Since the fit is, at best, only sensitive to $f(\mathbf{g})$, one can only meaningfully discriminate UV parameters \mathbf{g} that map to different points in the EFT parameter space W under the matching relation f . Thus, we

define ‘‘UV invariants’’ as those combinations of UV parameters such that f remains invariant under a mapping h , defined as

$$h : U \rightarrow I, \quad (2.15)$$

such that $f(h(\mathbf{g})) = f(h(\mathbf{g}'))$. We denote by I the space of UV invariants that is now bijective with W under f and that contains all the information that we can extract about the UV couplings by measuring f from experimental data in the global EFT fit.

To illustrate the role of UV invariants, we consider again the tree-level matching relations for our benchmark model Eq. (2.1) given by Eq. (2.2). Expressing the UV couplings in terms of the EFT coefficients leads to two different solutions,

$$(y_\phi^d)_{33} = -\sqrt{-\left(c_{qd}^{(8)}\right)_{3333} \frac{m_\phi}{\Lambda}}, \quad (y_\phi^u)_{33} = -\frac{c_{t\varphi}}{c_{b\varphi}} \sqrt{-\left(c_{qd}^{(8)}\right)_{3333} \frac{m_\phi}{\Lambda}}, \quad \lambda_\phi = \frac{c_{b\varphi}}{\sqrt{-\left(c_{qd}^{(8)}\right)_{3333}}} \frac{m_\phi}{\Lambda}, \quad (2.16)$$

and

$$(y_\phi^d)_{33} = \sqrt{-\left(c_{qd}^{(8)}\right)_{3333} \frac{m_\phi}{\Lambda}}, \quad (y_\phi^u)_{33} = \frac{c_{t\varphi}}{c_{b\varphi}} \sqrt{-\left(c_{qd}^{(8)}\right)_{3333} \frac{m_\phi}{\Lambda}}, \quad \lambda_\phi = -\frac{c_{b\varphi}}{\sqrt{\left(c_{qd}^{(8)}\right)_{3333}}} \frac{m_\phi}{\Lambda}, \quad (2.17)$$

where we have omitted the flavour indices of the coefficients for clarity. The resulting sign ambiguity stems from the sensitivity to the sign of only two products of the three UV couplings. Other non-vanishing EFT coefficients do not enter these solutions since they are related to the present ones via linear or non-linear relations.

Eqns. (2.16) and (2.17) hence indicate that the EFT fit is not sensitive to the sign of these UV couplings for this specific model. The sought-for mapping h between the original UV couplings $((y_\phi^d)_{33}, (y_\phi^u)_{33}, \lambda_\phi)$ and the UV invariants which can be meaningfully constrained by the global EFT fit is given by

$$h : ((y_\phi^d)_{33}, (y_\phi^u)_{33}, \lambda_\phi) \mapsto \left(|(y_\phi^u)_{33}|, \lambda_\phi \operatorname{sgn}((y_\phi^u)_{33}), (y_\phi^d)_{33} \operatorname{sgn}(\lambda_\phi) \right), \quad (2.18)$$

with $\operatorname{sgn}(x)$ being the sign function. Notice the degree of arbitrariness present in this construction, since for example one could have also chosen $(|\lambda_\phi|, (y_\phi^u)_{33} \operatorname{sgn}(\lambda_\phi))$ instead of the first two invariants of Eq. (2.18). This simple example displays only a sign ambiguity, but one could be unable to distinguish two UV couplings altogether since, e.g. they always appear multiplying each other. The `MATCH2FIT` package automates the computation of the transformations h defining the UV-invariants for the models at the tree-level matching level, see App. B for more details.

Furthermore, one can also illustrate the concept of UV-invariants by fitting the heavy scalar doublet model of Eq. (2.1) to the experimental data by following the procedure which will be outlined in Sect. 3. Fig. 2.1 shows the resulting marginalised posterior distributions in the space U of UV parameters $((y_\phi^u)_{33}, \lambda_\phi)$ and in the space I of UV invariants $(|(y_\phi^u)_{33}|, \lambda_\phi \operatorname{sgn}((y_\phi^u)_{33}))$. The red points indicate two different sets of UV couplings in U , $\mathbf{g} \neq \mathbf{g}'$, that are mapped to the same point in I upon the transformation h . Presenting results at the level of UV-invariants has the benefit of making explicit the symmetries and relations between UV-couplings that may be hidden otherwise if one presents results in the UV parameters space U . It is worth stressing that UV invariants do not necessarily correspond to combinations of UV parameters that one can constrain in a fit. Rather, they represent what can be said about the UV couplings from given values for the WCs and hence serve to map out the UV parameter space such that no redundant information is shown.

3 Implementation in SMEFIT

Here we describe how the SMEFIT global analysis framework [19–23] has been extended to operate, in addition to at the level of Wilson coefficients, directly at the level of the parameters of UV-complete

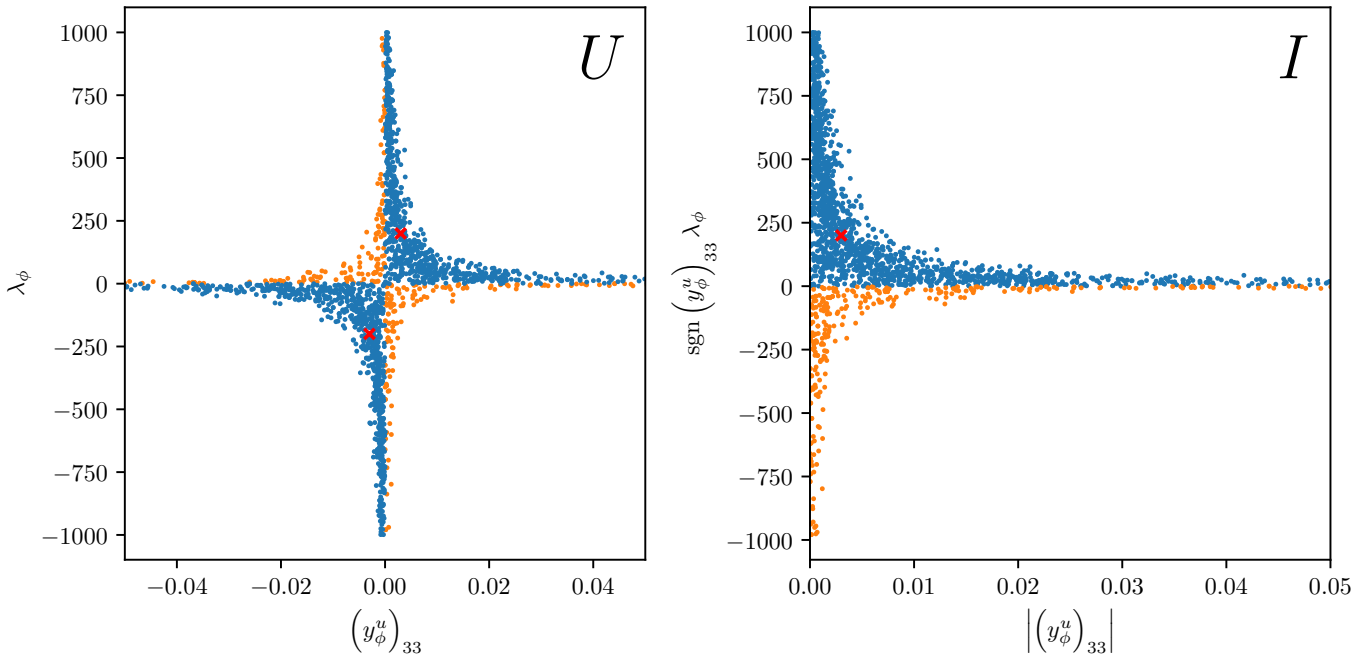


Figure 2.1: Left: marginalised posterior distributions in the space U of UV parameters $\left(\left(y_\phi^u\right)_{33}, \lambda_\phi\right)$ in the heavy scalar doublet model given by Eq. (2.1) fitted to the data according to the procedure of Sect. 3. Right: the same results represented in the space I of UV invariants $\left(\left|y_\phi^u\right|_{33}, \lambda_\phi \operatorname{sgn}\left(\left(y_\phi^u\right)_{33}\right)\right)$. The red points indicate two different sets of UV couplings in U that are mapped to the same point in I upon the transformation h . Blue (orange) points indicate positive (negative) values of the UV-invariant $\lambda_\phi \operatorname{sgn}\left(\left(y_\phi^u\right)_{33}\right)$.

models. We also present the baseline SMEFT analysis which will be used in Sect. 4 to constrain these UV parameters, reporting on a number of improvements as compared to its most recent version presented in [23], in particular concerning the implementation of precision electroweak observables (EWPOs) from the LEP legacy measurements. App. A provides additional details about the SMEFT functionalities and this baseline EFT global fit.

Assume a UV-complete model defined by the Lagrangian $\mathcal{L}_{\text{UV}}(\mathbf{g})$ which contains n_{UV} free parameters \mathbf{g} . Provided that this model has the SM as its low-energy limit with linearly realised electroweak symmetry breaking, one can derive matching relations between the SMEFT coefficients and the UV couplings of the form $\mathbf{c} = \mathbf{f}(\mathbf{g}, \mu)$ for a given choice of the matching scale μ as discussed in Sect. 2. Once these matching conditions are evaluated, the EFT cross-sections $\sigma(\mathbf{c})$ entering the fit can be expressed in terms of the UV couplings and masses $\sigma(\mathbf{f}(\mathbf{g}, \mu))$. By doing so, one ends up with the likelihood function L now expressed in terms of UV couplings, $L(\mathbf{g})$. Bayesian sampling techniques can now be applied directly to $L(\mathbf{g})$, assuming a given prior distribution of the UV coupling space, in the same manner as for the fit of EFT coefficients.

The current release of SMEFT enables the user to impose these matching conditions $\mathbf{c} = \mathbf{f}(\mathbf{g}, \mu)$ via run cards thanks to its support for a wide class of different constraints on the fit parameters, see App. A. The code applies the required substitutions on the theoretical predictions for the observables entering the fit automatically. Additionally, the availability of Bayesian sampling means that the functional relationship between the likelihood function L and the fitted parameters \mathbf{g} is unrestricted.

In order to carry out parameter inference directly at the level of UV couplings within SMEFT, three main ingredients are required:

- First, the matching relations \mathbf{f} between the parameters of the UV Lagrangian $\mathcal{L}_{\text{UV}}(\mathbf{g})$ and the EFT Wilson coefficients, $\mathbf{c} = \mathbf{f}(\mathbf{g})$ in the Warsaw basis used in the fit. As discussed in Sect. 2, this step can be achieved automatically both for tree-level and for one-loop matching relations by using MATCHMAKEREFT [12]. Other matching frameworks may also be used in this step.

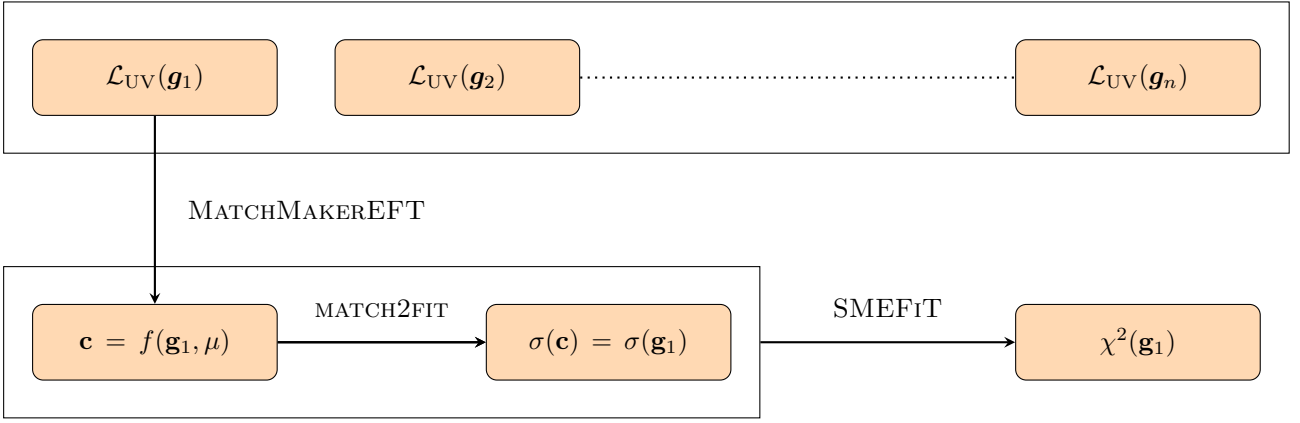


Figure 3.1: Schematic representation of the pipeline adopted in this work to map the parameter space of UV-complete models using the SMEFT as a bridge to the data. The starting point is a UV-Lagrangian containing a number of free parameters \mathbf{g} such as its masses and coupling constants, for which a flat prior is assumed. We then determine the matching relations between the UV parameters \mathbf{g} and the corresponding EFT coefficients \mathbf{c} at the matching scale μ using `MATCHMAKEREFT`. Then the `MATCH2FIT` interface enables expressing cross-sections for processes entering the EFT in terms of the UV-parameters \mathbf{g} . Finally, these UV-parameters are constrained from the data using the sampling methods of `SMEFIT` applied to the figure of merit $\chi^2(\mathbf{g})$ evaluated on a global dataset.

- Second, the conversion between the output of the matching code, `MATCHMAKEREFT` in our case, and the input required for the `SMEFIT` run cards specifying the dependence of the Wilson coefficients \mathbf{c} on the UV couplings \mathbf{g} such that the replacement $\sigma(\mathbf{c}) \rightarrow \sigma(\mathbf{f}(\mathbf{g}))$ on the physical observables entering the fit can be implemented. For this we use the new Mathematica package `MATCH2FIT` summarised in App. B. The automation of this step is currently limited to tree-level matching results. `SMEFIT` then performs the replacements $\sigma(\mathbf{c}) \rightarrow \sigma(\mathbf{f}(\mathbf{g}))$ specified by the runcards.
- Third, a choice of prior volume in the space U spanned by the UV couplings \mathbf{g} entering the fit. In this work, we assume a flat prior on the UV parameters \mathbf{g} and verify that results are stable with respect to variations of this prior volume. We note that, for the typical (polynomial) matching relations between UV couplings and EFT coefficients, this choice of prior implies non-trivial forms for the priors on the space of the latter. This observation is an important motivation to support the choice of fitting directly at the level of UV couplings.

Once these ingredients are provided, `SMEFIT` performs the global fit by comparing EFT theory predictions with experimental data and returning the posterior probability distributions on the space of UV couplings \mathbf{g} or any combination thereof. Fig. 3.1 displays a schematic representation of the pipeline adopted in this work to map in an automated manner the parameter space of UV-complete models using the SMEFT as a bridge to the data and based on the combination of three tools: `MATCHMAKEREFT` to derive the matching relations, `MATCH2FIT` to transform its output into the `SMEFIT`-compliant format, and `SMEFIT` to infer from the data bounds on the UV coupling space.

Concerning the UV-invariants introduced in Sect. 2.3, we should note here that depending on the specific UV-complete model, one might be able to constrain only the absolute value of certain UV parameters or of their product. For this reason, here we will display results mostly at the level of UV-invariants $I_{UV}(\mathbf{g})$ determined from the matching relations. We will find that certain UV-invariants may nevertheless remain unconstrained, due to the lack of sensitivity to specific EFT coefficients in the fitted data. In any case, the user can easily define arbitrary combinations of the UV parameters to be fitted to the data.

The baseline global `SMEFIT` analysis adopted in this work to constrain the parameter space of UV-complete models is based on the analysis presented in [23], which in turn updated the global SMEFT

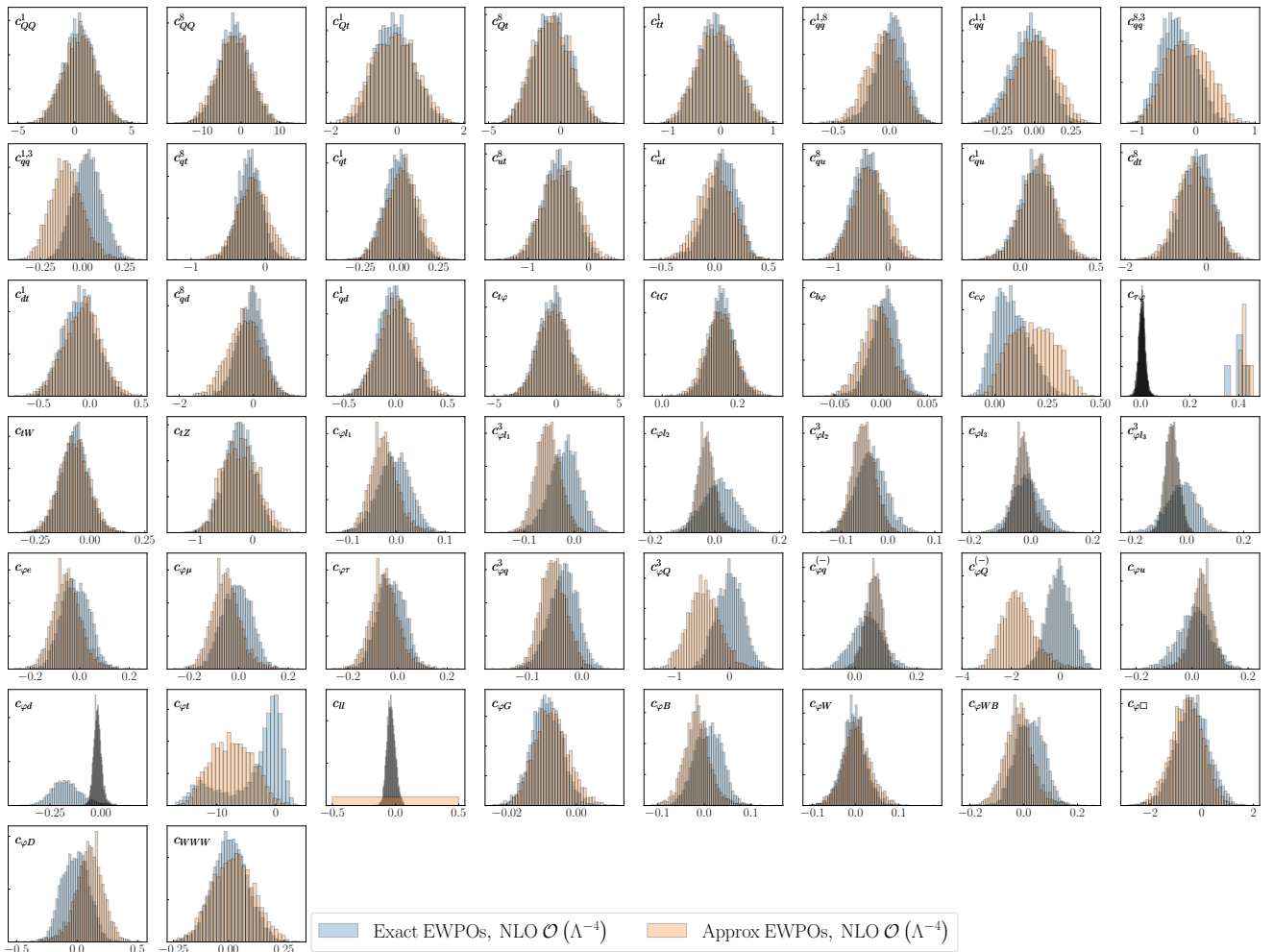


Figure 3.2: Marginalised single-parameter posterior probability distributions in the global SMEFT fit of [23], based on an approximate implementation of the EWPOs, compared with the baseline fit adopted in this work and implementing the EWPOs constraints in an exact manner. Note that the results labelled as “Approx EWPOs” differ slightly from those in [23] due to the use of updated theory predictions for LHC processes, see text. In both cases, the fits include quadratic EFT effects and NLO QCD corrections to the EFT cross-sections.

analysis of Higgs, top quark, and diboson data from [22]. In comparison with [23], a significant upgrade is the new implementation of the information provided by the legacy EWPOs [35] from LEP and SLC in the Wilson coefficients. Previously, the constraints provided by these EWPOs in the SMEFT parameter space were accounted in an approximate manner, assuming EWPOs measured with vanishing uncertainties.¹

As a consequence of this improvement, the present global SMEFT analysis considers 14 additional Wilson coefficients \mathbf{c} with respect to the basis used in [22, 23], leading to a total of 50 independent parameters constrained from the data. Since these new degrees of freedom are constrained not only by the EWPOs, but also by LHC observables, we have recomputed all EFT cross-sections for those processes where such operators enter. As in the original analysis [22], we use `MG5_AMC@NLO` [37] interfaced to `SMEFT@NLO` [38] to evaluate linear and quadratic EFT corrections which account up to NLO QCD perturbative corrections, whenever available. A dedicated description of this new implementation of the EWPOs in `SMEFT` and of their phenomenological implications for present and future colliders will be discussed in a forthcoming publication [39].

¹For the purposes of benchmarking with the ATLAS EFT analysis of [36], in [23] also fits with EWPOs were considered, but these were based on the exact same theory inputs as in the ATLAS paper.

The impact of this new exact EWPOs implementation is illustrated in Fig. 3.2, comparing the marginalised one-parameter posterior distributions obtained in the global SMEFT fit of [23] and based on the approximate EWPOs implementation, with the baseline fit adopted in this work where EWPOs are taken into account in an exact manner. Note that the results labelled as “Approx EWPOs” differ slightly from those in [23] due to the use of updated theory predictions. In both cases, the fits include quadratic EFT effects and NLO QCD corrections to the EFT cross-sections.

In general, there is good agreement at the level of Wilson coefficients between results based on the approximate and the exact implementation of the EWPOs, with some noticeable differences. While the posterior distributions for most operators are only moderately affected by the EWPOs, their impact is visible for some of the coefficients affecting electroweak interactions such as $c_{\phi t}$ (where a new double-peak structure is revealed), $(c_{\ell\ell})_{1111}$ (which was previously unconstrained), $c_{\phi d}$, $c_{\phi Q}^{(3)}$, and $c_{\phi Q}^{(-)}$. Nevertheless, differences between exact and approximate implementation of EWPOs, which will be further studied in [39], are well contained within the respective 95% CL intervals.

4 Results

We now present the main results of this work, namely the constraints on the parameter space of a broad range of UV-complete models obtained using the SMEFT global analysis integrated with the pipeline described in Sects. 2 and 3. We discuss the following results in turn: one-particle models matched at tree level, multi-particle models also matched at tree level, and one-particle models matched at the one-loop level. For each category of models, we study both the impact of linear and quadratic corrections in the SMEFT expansion as well as of the QCD accuracy. Whenever possible, we provide comparisons with related studies to validate our results.

The UV models considered in this work are composed of one or more of the heavy BSM particles listed in Table 4.1 and classified in terms of their spin as scalar, fermion, and vector particles. For each particle, we indicate the irreducible representation of the SM gauge group under which they transform. These particles can couple linearly to the SM fields and hence generate dimension-6 SMEFT operators after being integrated out at tree level. The complete tree-level matching results for these particles were computed in [3], from where we adopt the notation. The only exception is the heavy scalar field φ , which we rename ϕ to be consistent with the convention used in Sect. 2.

Concerning one-particle models, we include each of the particles listed in Table 4.1 one at the time, and then impose restrictions on the couplings between the UV heavy fields and the SM particles such that these models satisfy the SMEFT flavour assumption after matching at tree level. A discussion on the UV couplings allowed for each of the considered models under such restriction can be found in App. D. We have discarded from our analysis those heavy particles considered in [3] for which we could not find a set of restrictions on their UV couplings such that they obeyed the baseline EFT fit flavour assumptions.

With regard to multi-particle models, we consider combinations of the one-particle models mentioned above without additional assumptions on their UV couplings unless specified. For illustration purposes, we will present results for the model that results from adding the custodially-symmetric models with vector-like fermions and an $SU(2)_L$ triplet vector boson, presented in [40]. We analyse the cases of both degenerate and different heavy particle masses.

An overview of which Wilson coefficients are generated by each UV particle at tree level is provided in Table 4.2 for heavy scalars and vector bosons and in Table 4.3 for heavy vector-like fermions. Black ticks indicate the EFT coefficients probed when applying the SMEFT flavour restrictions, while red ones indicate those probed only when the flavour-universal UV couplings assumption of the FITMAKER analysis [16] is used. Notice that some operators are not generated by any of the models considered in this work, e.g. four-fermion operators with two-light and two-heavy quarks or with purely light-quark ones. This is due, in part, to the correlations among operators imposed by UV models and the restrictions imposed by the

Scalars		Fermions		Vectors	
Particle	Irrep	Particle	Irrep	Particle	Irrep
\mathcal{S}	$(1, 1)_0$	N	$(1, 1)_0$	\mathcal{B}	$(1, 1)_0$
\mathcal{S}_1	$(1, 1)_1$	E	$(1, 1)_{-1}$	\mathcal{B}_1	$(1, 1)_1$
ϕ	$(1, 2)_{1/2}$	Δ_1	$(1, 2)_{-1/2}$	\mathcal{W}	$(1, 3)_0$
Ξ	$(1, 3)_0$	Δ_3	$(1, 2)_{-3/2}$	\mathcal{W}_1	$(1, 3)_1$
Ξ_1	$(1, 3)_1$	Σ	$(1, 3)_0$	\mathcal{G}	$(8, 1)_0$
ω_1	$(3, 1)_{-1/3}$	Σ_1	$(1, 3)_{-1}$	\mathcal{H}	$(8, 3)_0$
ω_4	$(3, 1)_{-4/3}$	U	$(3, 1)_{2/3}$	\mathcal{Q}_5	$(8, 3)_0$
ζ	$(3, 3)_{-1/3}$	D	$(3, 1)_{-1/3}$	\mathcal{Y}_5	$(\bar{6}, 2)_{-5/6}$
Ω_1	$(6, 1)_{1/3}$	Q_1	$(3, 2)_{1/6}$		
Ω_4	$(6, 1)_{4/3}$	Q_7	$(3, 2)_{7/6}$		
Υ	$(6, 3)_{1/3}$	T_1	$(3, 3)_{-1/3}$		
Φ	$(8, 2)_{1/2}$	T_2	$(3, 3)_{2/3}$		
		Q_5	$(3, 2)_{-5/6}$		

Table 4.1: Heavy BSM particles entering the UV-complete models considered in this work. For each particle, we indicate the irreducible representation of the SM gauge group under which they transform, with notation $(\text{SU}(3)_c, \text{SU}(2)_L)_{\text{U}(1)_Y}$.

assumed flavour symmetry. We recall that, in general, one-loop matching will introduce more coefficients as compared to the tree-level ones listed in Tables 4.2 and 4.3

Finally, we will consider the model composed of a heavy scalar doublet ϕ matched to the SMEFT at the one-loop level. In this case, we impose the SMEFT flavour restriction only at tree level. The operators generated by this model at one-loop were already discussed in Sect. 2.2.

In the following, confidence level (CL) intervals for the UV model parameters are evaluated as highest density intervals (HDI or HPDI) [41]. The HDI is defined as the interval such that all values inside the HDI have higher probability than any value outside. In contrast to equal-tailed intervals (ETI) which are based on quantiles, HDI does not suffer from the property that some value inside the interval might have lower probability than the ones outside the interval. Whenever the lower bound is two orders of magnitude smaller than the width of the CL interval, we round it to zero.

4.1 One-particle models matched at tree level

Here we present results obtained from the tree-level matching of one-particle extensions of the SM. Motivated by the discussion in Sect. 2.3, we present results at the level of UV invariants since these are the combinations of UV couplings that are one-to-one with the Wilson coefficients under the matching relations. We study in turn the one-particle models containing heavy scalars, fermions, and vector bosons listed in Tables 4.2 and 4.3. We also present a comparison with the one-particle models considered in the FITMAKER analysis [16].

Heavy scalars. The upper part of Table 4.4 shows the 95% CL intervals obtained for the UV invariants associated to the one-particle heavy scalar models considered in this work and listed in Table 4.1. We compare results obtained with different settings of the global SMEFT fit: linear and quadratic level in

	Heavy Scalars												Heavy Vector Bosons									
	\mathcal{S}	\mathcal{S}_1	ϕ	Ξ	Ξ_1	ω_1	ω_4	ζ	Ω_1	Ω_4	Υ	Φ	\mathcal{B}	\mathcal{B}_1	\mathcal{W}	\mathcal{W}_1	\mathcal{G}	\mathcal{H}	\mathcal{Q}_5	\mathcal{Y}_5	$\mathcal{B}_1\mathcal{B}$	
$c_{\varphi\Box}$	✓			✓	✓								✓	✓	✓	✓						✓
$c_{\varphi D}$				✓	✓								✓	✓		✓						
$c_{\mathcal{T}\varphi}$			✓	✓	✓									✓	✓	✓						✓
$c_{b\varphi}$			✓	✓	✓									✓	✓	✓						✓
$c_{t\varphi}$			✓	✓	✓									✓	✓	✓						✓
$c_{\varphi l_{1,2,3}}^{(3)}$															✓							
$c_{\varphi l_{1,2,3}}^{(1)}$													✓									
$c_{\varphi(e,\mu,\tau)}$													✓									
$c_{\varphi Q}^{(3)}$															✓							
$c_{\varphi Q}^{(-)}$													✓		✓							
$c_{\varphi q}^{(3)}$																						
$c_{\varphi t}$													✓									
$c_{\ell\ell}$		✓													✓							
c_{Qt}^1			✓									✓	✓							✓	✓	
c_{Qt}^8			✓									✓					✓			✓	✓	
c_{QQ}^1						✓		✓	✓		✓	✓		✓	✓			✓				
c_{QQ}^8						✓		✓	✓		✓	✓		✓	✓		✓	✓				
c_{tt}^1							✓			✓		✓					✓					
$c_{qd}^{(1)\dagger}$			✓																			
$c_{qd}^{(8)\dagger}$			✓																			
$c_{\ell\ell_{1111}}$													✓		✓							

Table 4.2: The Wilson coefficients, in the SMEFIT fitting basis, generated at tree level by the heavy scalar and vector boson particles whose quantum numbers are listed in Table 4.1. Particles highlighted in red corresponds to one-particle models also considered in the FITMAKER analysis [16]. Red check marks indicate operators relevant for the flavor assumptions of [16]. Coefficients marked with \dagger correspond to operators generated by the heavy scalar model ϕ in [16] restricted to the third quark generation. In our analysis, we take such a flavour-universal restriction exclusively when comparing our results with those from [16].

the EFT expansion and either LO or NLO QCD accuracy for the EFT cross-sections. We exclude from Table 4.4 the results of heavy scalar model ϕ that is characterised by two UV invariants. In all cases, we assume that the mass of the heavy particle is $m_{UV} = 1$ TeV, and hence all the UV invariants shown are dimensionless. The resulting bounds for these heavy scalar models are well below the naive perturbative limit $g \lesssim 4\pi$ in most cases, and only for a few models in linear EFT fits the bounds are close to saturate the perturbative unitarity condition, $g \lesssim \sqrt{8\pi}$ [42].

Comparing the impact of linear versus quadratic corrections, we notice a significant improvement in sensitivity for the heavy scalar models ω_1 , ω_4 , ζ , Ω_1 , Ω_4 , Υ and Φ . This can be explained by the fact that they generate four-fermion operators, as these are characterised by large quadratic corrections. Indeed, four-heavy operators, constrained in the EFT fit by $t\bar{t}t\bar{t}$ and $t\bar{t}b\bar{b}$ cross-section data, have limited sensitivity in the linear EFT fit. In the remaining models, the impact of quadratic EFT corrections on the UV-invariant bounds is small. Considering the impact of the QCD perturbative accuracy used for the EFT cross-sections, one notices a moderate improvement of $\sim 10\%$ for models that are sensitive to four-fermion

	Heavy Fermions											
	N	E	Δ_1, Δ_3	Σ, Σ_1	U	D	Q_1	Q_5	Q_7	T_1, T_2	T	Q_{17}
$c_{\varphi l_1}^{(3)\dagger}$	✓	✓		✓								
$c_{\varphi l_1}^{\dagger}$	✓	✓		✓								
$c_{\varphi l_2}^{(3)\dagger}$	✓	✓		✓								
$c_{\varphi l_2}^{\dagger}$	✓	✓		✓								
$c_{\varphi l_3}^{(3)\dagger}$	✓	✓		✓								
$c_{\varphi l_3}^{\dagger}$	✓	✓		✓								
$c_{\varphi \tau}^{\dagger}$			✓									
$c_{\varphi(e,\mu)}^{\dagger}$			✓									
$c_{\tau\varphi}$		✓	✓	✓								
$c_{\varphi Q}^{(3)\dagger}$					✓	✓				✓	✓	
$c_{\varphi Q}^{(-)\dagger}$					✓					✓	✓	
$c_{\varphi t}$							✓		✓			
$c_{t\varphi}$					✓		✓		✓	✓	✓	✓
$c_{b\varphi}$						✓		✓		✓		
$c_{\varphi q}^{(3)\dagger}$					✓	✓				✓		
$c_{\varphi q}^{(-)\dagger}$					✓					✓		
$c_{\varphi d_i}$								✓				
$c_{\varphi u_i}$									✓			

Table 4.3: Same as Table 4.2 for the heavy fermions. Coefficients labelled with \dagger correspond to operators probed in [16] in a flavour-universal way, i.e. it is assumed that $c_{\varphi l_{1,2,3}}^{(3)} = c_{\varphi l}^{(3)}$ and likewise for the others. In our analysis, we take such a flavour-universal restriction exclusively when benchmarking our results against those from [16].

operators with the exception of ω_1 .

The posterior distributions associated to the heavy scalar models listed in Table 4.4 are shown in Figs. 4.1 and 4.2, comparing results with different EFT expansion order and QCD accuracy respectively. To facilitate visualisation of the bulk region, the distributions are cut after the distribution has dropped to 5% of its maximum, though this choice is independent from the calculation of the CL bounds. One can see how using quadratic EFT corrections (NLO QCD cross-sections) improve significantly (moderately) the bounds on models that are sensitive to four-fermion operators for the reasons mentioned above. For all models considered, the posterior distributions indicate agreement with the SM, namely vanishing UV model couplings.

Along the same lines, from Figs. 4.1 and 4.2 one also observes that the posterior distributions of the absolute values of UV couplings tend to exhibit a most likely value (mode) away from zero. This feature is not incompatible with a posterior distribution on the EFT coefficient space that favours the SM case. The reason is that when transforming the probability density function from one space to the other, one must consider the Jacobian factor that depends on the functional relation between EFT coefficients and UV couplings. For most matching relations, this Jacobian factor can generate these peaks away from zero in the UV coupling space even when the EFT fit favours the SM solution.

Model	UV invariants	LO $\mathcal{O}(\Lambda^{-2})$	LO $\mathcal{O}(\Lambda^{-4})$	NLO $\mathcal{O}(\Lambda^{-2})$	NLO $\mathcal{O}(\Lambda^{-4})$
\mathcal{S}	$ \kappa_{\mathcal{S}} $	[0, 1.4]	[0, 1.4]	[0, 1.5]	[0, 1.4]
\mathcal{S}_1	$(y_{\mathcal{S}_1})_{12} (y_{\mathcal{S}_1})_{21}$	[-0.041, 0.0018]	[-0.040, 0.0042]	[-0.042, 0.0027]	[-0.042, 0.0030]
Ξ	$ \kappa_{\Xi} $	[0, 0.067]	[0, 0.069]	[0, 0.069]	[0, 0.069]
Ξ_1	$ \kappa_{\Xi_1} $	[0, 0.049]	[0, 0.049]	[0, 0.049]	[0, 0.048]
ω_1	$ (y_{\omega_1}^{qq})_{33} $	[0, 5.0]	[0, 1.6]	[0, 5.2]	[0, 1.7]
ω_4	$ (y_{\omega_4}^{uu})_{33} $	[0.027, 3.6]	[0.021, 1.1]	[0, 3.1]	[0.043, 1.0]
ζ	$ (y_{\zeta}^{qq})_{33} $	[0.11, 3.7]	[0.011, 1.0]	[0.14, 3.3]	[0.034, 0.99]
Ω_1	$ (y_{\Omega_1}^{qq})_{33} $	[0.021, 4.4]	[0, 1.5]	[0, 4.0]	[0.031, 1.4]
Ω_4	$ (y_{\Omega_4})_{33} $	[0.099, 5.165]	[0.059, 1.553]	[0, 4.4]	[0.037, 1.4]
Υ	$ (y_{\Upsilon})_{33} $	[0, 3.4]	[0, 1.1]	[0, 3.0]	[0.027, 1.0]
Φ	$ (y_{\Phi}^{qu})_{33} $	[0.14, 11]	[0, 2.9]	[0.018, 9.8]	[0.014, 2.6]
N	$ \lambda_N^e _3$	[0, 0.47]	[0, 0.47]	[0, 0.47]	[0, 0.48]
E	$ \lambda_E _3$	[0, 0.24]	[0, 0.25]	[0, 0.25]	[0, 0.25]
Δ_1	$ \lambda_{\Delta_1} _3$	[0, 0.21]	[0, 0.20]	[0, 0.21]	[0, 0.20]
Δ_3	$ \lambda_{\Delta_3} _3$	[0, 0.26]	[0, 0.27]	[0.0015, 0.26]	[0, 0.27]
Σ	$ \lambda_{\Sigma} _3$	[0, 0.29]	[0, 0.28]	[0, 0.28]	[0, 0.29]
Σ_1	$ \lambda_{\Sigma_1} _3$	[0, 0.42]	[0, 0.42]	[0, 0.43]	[0, 0.42]
U	$ \lambda_U _3$	[0, 0.84]	[0, 0.85]	[0, 0.82]	[0, 0.84]
D	$ \lambda_D _3$	[0, 0.23]	[0, 0.24]	[0, 0.24]	[0, 0.23]
Q_1	$ \lambda_{Q_1}^u _3$	[0, 0.94]	[0, 0.95]	[0, 0.93]	[0, 0.92]
Q_7	$ \lambda_{Q_7} _3$	[0, 0.95]	[0, 0.93]	[0, 0.91]	[0, 0.91]
T_1	$ \lambda_{T_1} _3$	[0, 0.46]	[0, 0.46]	[0, 0.45]	[0, 0.47]
T_2	$ \lambda_{T_2} _3$	[0, 0.39]	[0, 0.38]	[0, 0.38]	[0, 0.38]

Table 4.4: The 95% CL intervals for the UV invariants relevant for the heavy scalar (upper part) and heavy fermion (lower part of the table) one-particle models matched at tree-level. We quote the 95% CL upper limit and the lower limit is rounded to 0 whenever it is two orders of magnitudes smaller than the total CL width. For each model we compare results obtained at the linear and quadratic level in the EFT expansion and using either LO or NLO perturbative QCD corrections to the EFT cross-sections. In all cases, we set the mass of the heavy particle to $m_{UV} = 1$ TeV. Note that the model with heavy scalar ϕ is considered separately in Table 4.5, given that it is parameterised in terms of multiple UV invariants.

To illustrate this somewhat counter-intuitive result, consider a toy model for the probability density of a (positive-definite) Wilson coefficient c ,

$$P(c) = \frac{2}{\sqrt{\pi}} e^{-c^2}, \quad \int_0^{\infty} dc P(c) = 1, \quad (4.1)$$

where the underlying law is the SM. For a typical matching condition of the form $c = g^2$, (see i.e. the heavy scalar model of Eq. (2.2)), the transformed probability distribution for the ‘‘UV-invariant’’ $|g|$ is

$$P(|g|) = \frac{4}{\sqrt{\pi}} |g| e^{-|g|^4}, \quad \int_0^{\infty} d|g| P(|g|) = 1, \quad (4.2)$$

which is maximised by $g = 1/\sqrt{2} \neq 0$. Hence posterior distributions in the UV coupling space favouring non-zero values do not (necessarily) indicate preference for BSM solutions in the fit. On the other hand,

Model	UV invariants	LO $\mathcal{O}(\Lambda^{-2})$	LO $\mathcal{O}(\Lambda^{-4})$	NLO $\mathcal{O}(\Lambda^{-2})$	NLO $\mathcal{O}(\Lambda^{-4})$
ϕ (tree-level)	$ \lambda_\phi $	$[0, 8.2 \cdot 10^2]$	$[0, 7.4 \cdot 10^2]$	$[0, 8.0 \cdot 10^2]$	$[0, 7.9 \cdot 10^2]$
	$\text{sgn}(\lambda_\phi) \left(y_\phi^u\right)_{33}$	$[-0.11, 1.0]$	$[-0.20, 2.1]$	$[-0.19, 0.62]$	$[-0.18, 1.7]$
ϕ (one-loop)	$ \lambda_\phi $	$[0, 7.6]$	$[0, 7.6]$	$[0, 7.6]$	$[0, 7.1]$
	$\text{sgn}(\lambda_\phi) \left(y_\phi^u\right)_{33}$	$[-0.81, 2.8]$	$[-1.2, 2.3]$	$[-0.80, 2.2]$	$[-0.87, 2.1]$

Table 4.5: Same as Table 4.4 for the heavy scalar ϕ model, which has associated two independent UV-invariants. See Fig. 4.3 for the associated posterior distributions.

posteriors on the UV that are approximately constant near zero correspond to posteriors in the WC space that diverge towards zero.

One also observes from Table 4.4 that two of the considered heavy scalar models, specifically those containing the Ξ and Ξ_1 particles, lead to bounds which are at least two orders of magnitude more stringent than for the rest. These two models generate the same operators with slightly different matching coefficients, and as indicated in Table 4.2 they are the only scalar particles that generate the Wilson coefficient $c_{\varphi D}$, which is strongly constrained by the EWPOs. Therefore, one concludes that the heavy scalar models with the best constraints are those whose generated operators are sensitive to the high-precision electron-positron collider data.

The heavy scalar models that we have discussed so far and listed in Table 4.4 depend on a single UV invariant. On the other hand, as discussed in Sect. 2.3, the heavy scalar ϕ model depends on two different UV couplings, λ_ϕ and $(y_\phi^u)_{33}$, resulting in two independent invariants. We present the corresponding 95% CL intervals from tree-level matching in the upper part of Table 4.5 and their distributions in Fig. 4.3. One finds that this model exhibits a degeneracy along the $(y_\phi^u)_{33} = 0$ direction, meaning that λ_ϕ can only be constrained whenever $(y_\phi^u)_{33} \neq 0$. This feature can be traced back to the tree-level matching relations in Eq. (2.2) with $(y_\phi^{d,e})_{33} = 0$ and the fact that there is no observable sensitive to the c_φ operator in the SMEFIT dataset as well as the fact that the data does not prefer a non-zero $(y_\phi^u)_{33}$. As we discuss below, this flat direction is lifted once one-loop corrections to the matching relations are accounted for. As opposed to the UV-invariants in Table 4.4, for this model the constrained UV-invariant is not positive-definite.

Heavy fermions. Following the discussion of the results for the single-particle BSM extensions with heavy scalars, we move to the corresponding analysis involving the heavy vector-like fermions listed in Table 4.1. We provide their 95% CL bounds in the lower part of Table 4.4, with the corresponding posterior distributions shown in Fig. 4.4. All the (positive-definite) UV-invariants can be constrained from the fit, leaving no flat directions, and are consistent with the SM hypothesis. One observes how the constraints achieved in all the heavy fermion models are in general similar, with differences no larger than a factor 4 depending on the specific gauge representation. Additionally, all the bounds are $\mathcal{O}(0.1)$, indicating that current data probes weakly-coupled fermions with masses around 1 TeV.

For these heavy fermion models, differences between fits carried out at the linear and quadratic levels in the EFT expansion are minimal. These reason is that these UV scenarios are largely constrained by the precisely measured EWPOs from LEP and SLC, composed by processes for which quadratic EFT corrections are very small [39]. The same considerations apply to the stability with respect to higher-order QCD corrections, which are negligible for the EWPOs.

Heavy vector bosons. The last category of single-particle models listed in Table 4.1 is the one composed of heavy vector bosons. We provide their 95% marginalised CL intervals in Table 4.6, with the corresponding posterior distributions in Fig. 4.5 in which we compare linear and quadratic EFT corrections at NLO QCD.

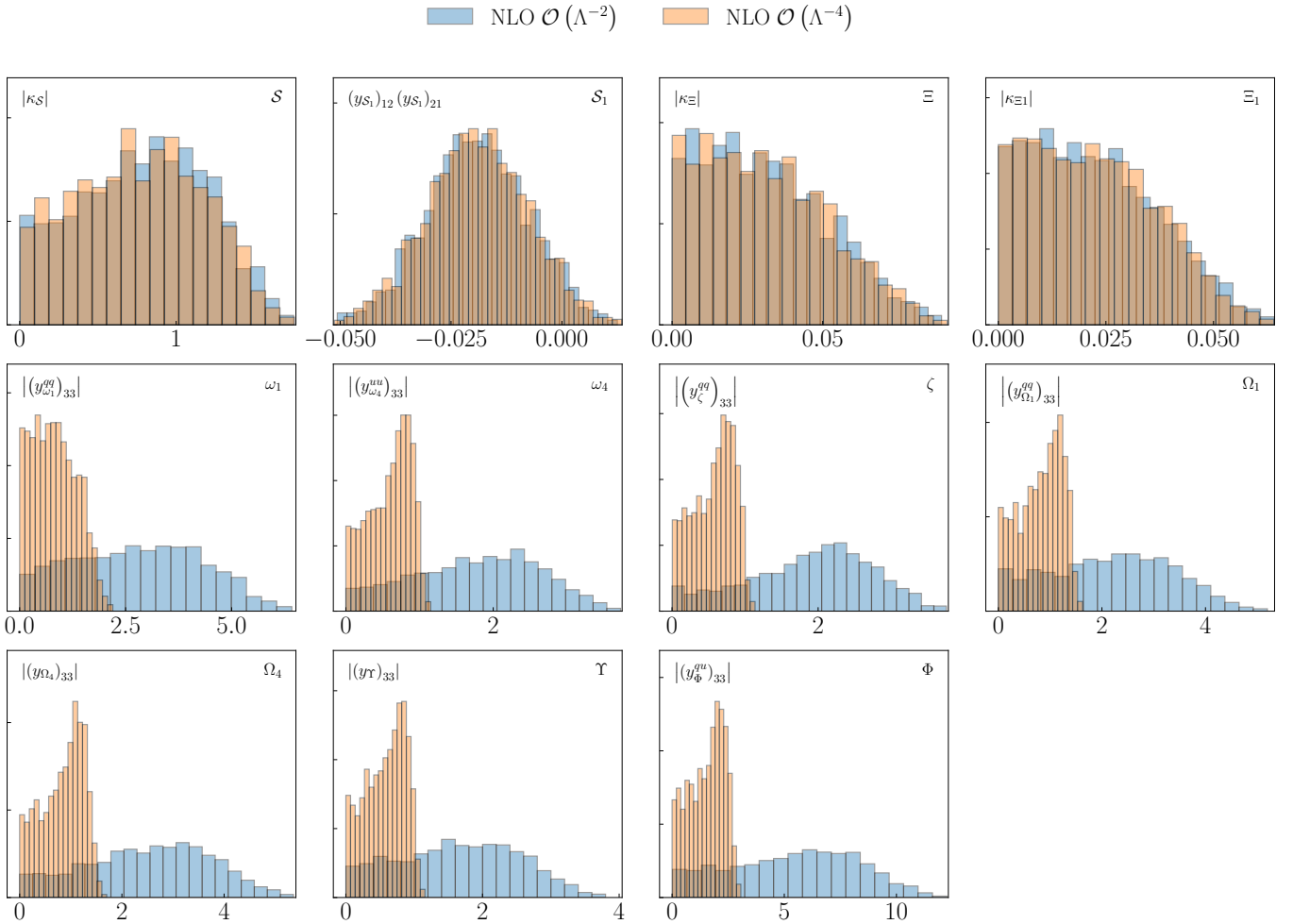


Figure 4.1: Posterior distributions associated to the UV-invariants in the one-particle heavy scalar models listed in the upper part of Table 4.4 and obtained from tree-level matching. Note that all UV-invariants for the considered models are positive-definite. We compare the results based on linear and quadratic corrections in the EFT expansion, in both cases with NLO QCD accuracy. To facilitate visualisation, the posterior distributions are cut after they have dropped to 5% of its maximum, though this does not affect the calculation of the bounds listed in Table 4.4.

A first observation is that most of the heavy vector models depend on multiple UV-invariants. To be specific, the \mathcal{B} , \mathcal{W} and \mathcal{G} vector models have associated 9, 5 and 2 UV-invariants respectively, while the other vector models are characterised by a single UV-invariant. For all models considered, results are consistent with the SM scenario, corresponding to vanishing UV parameters.

Regarding model \mathcal{B} , its results can be understood as follows. First of all, we observe a strong increase in sensitivity at the quadratic level in the last two invariants, $\text{sgn}(g_{\mathcal{B}}^{\varphi})(g_{\mathcal{B}}^q)_{33}$ and $\text{sgn}(g_{\mathcal{B}}^{\varphi})(g_{\mathcal{B}}^u)_{33}$. Indeed, they generate the four-heavy operators $c_{tt}^{(1)}$ and $c_{QQ}^{(1)}$, respectively, which are characterised by large quadratic corrections. The other UV-invariants in the \mathcal{B} model generate operators sensitive to the EWPOs which are strongly constrained from LEP data leading to strong bounds in all cases. For example, the operators $c_{\varphi\Box}$ and $c_{\varphi D}$ are generated by $g_{\mathcal{B}}^{\varphi}$,

$$\frac{c_{\varphi\Box}}{\Lambda^2} = \frac{1}{2} \frac{(g_{\mathcal{B}}^{\varphi})^2}{m_{\mathcal{B}}^2}, \quad \frac{c_{\varphi D}}{\Lambda^2} = -2 \frac{(g_{\mathcal{B}}^{\varphi})^2}{m_{\mathcal{B}}^2}, \quad (4.3)$$

and thus provide strong bounds on the invariant $|g_{\mathcal{B}}^{\varphi}|$. Furthermore, the invariant $(g_{\mathcal{B}}^e)_{ii} g_{\mathcal{B}}^{\varphi}$ is sensitive to the leptonic Yukawa operators $c_{\varphi(e,\mu,\tau)}$ and therefore gets well constrained by LEP data as well. Yet another example related to the EWPOs is the invariant $g_{\mathcal{B}}^{\varphi} (g_{\mathcal{B}}^{\ell})_{ii}$ that generates the operators $c_{\varphi\ell_2}$ and

■ LO $\mathcal{O}(\Lambda^{-4})$
 ■ NLO $\mathcal{O}(\Lambda^{-4})$

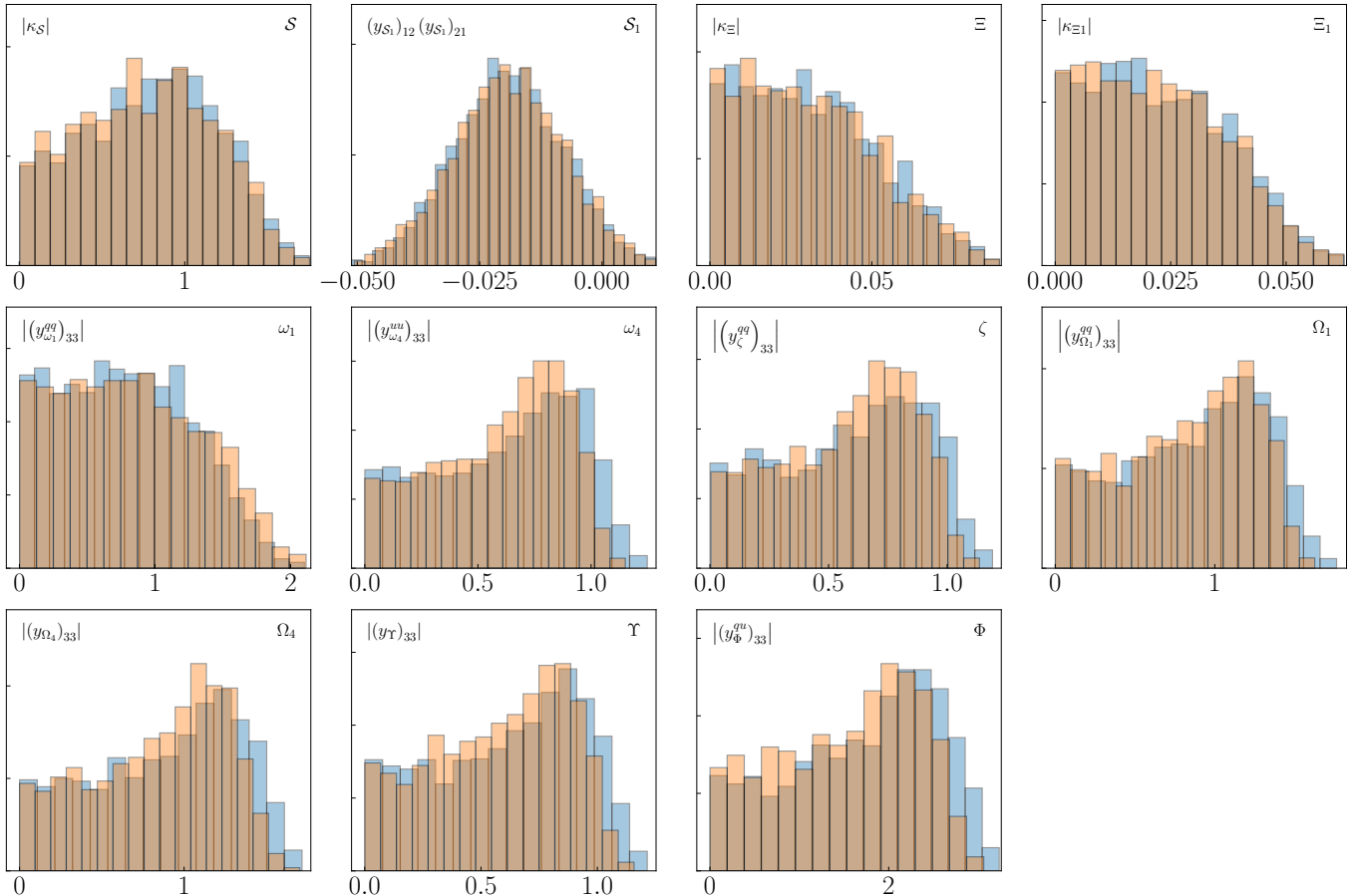


Figure 4.2: Same as Fig. 4.2, now comparing the baseline results, based on NLO QCD cross-sections for the EFT cross-sections, with the fit variant restricted to LO accuracy.

$c_{\varphi\ell_3}$ for $i = 1, 2$, respectively. Finally, $(g_{\mathcal{B}}^{\ell})_{11}$ generates $(c_{\ell\ell})_{1111}$ and thus gets constrained by Bhabha scattering. For this model, we have chosen the UV-invariants such that they agree with the constrained directions. Had we built them in the same way that for other models, it would be explicit that there are 5 poorly constrained directions along $|(g_{\mathcal{B}}^e)_{11}|$, $|(g_{\mathcal{B}}^e)_{22}|$, $|(g_{\mathcal{B}}^e)_{33}|$, $|(g_{\mathcal{B}}^{\ell})_{22}|$, and $|(g_{\mathcal{B}}^{\ell})_{33}|$. The model \mathcal{B}_1 is only sensitive to operators that can be constrained via EWPOs, hence no improved sensitivity is observed after adding quadratic EFT effects.

Moving on to model \mathcal{W} , we observe two flat directions along $(g_{\mathcal{W}}^{\ell})_{33}$ and $\text{sgn}((g_{\mathcal{W}}^{\ell})_{11})(g_{\mathcal{W}}^{\ell})_{22}$. In the matching relations, the UV coupling $(g_{\mathcal{W}}^{\ell})_{33}$ enters exclusively in a product together with $g_{\mathcal{W}}^{\varphi}$. Now, $g_{\mathcal{W}}^{\varphi}$ already gets strongly constrained via other independent relations to $c_{\varphi\Box}$, $c_{b\varphi}$, $c_{t\varphi}$ and $c_{\tau,\varphi}$. As a result, the UV invariant $|(g_{\mathcal{W}}^{\ell})_{33}|$ is left essentially unconstrained as no other matching relation exists to disentangle $(g_{\mathcal{W}}^{\ell})_{33}$ from $g_{\mathcal{W}}^{\varphi}$. A similar argument holds for the second flat direction we observe along $\text{sgn}((g_{\mathcal{W}}^{\ell})_{11})(g_{\mathcal{W}}^{\ell})_{22}$. The UV parameter $(g_{\mathcal{W}})_{22}$ only enters as a product with either $(g_{\mathcal{W}}^{\ell})_{11}$ or $g_{\mathcal{W}}^{\varphi}$, both of which already get constrained via other independent matching relations, e.g. $(c_{\ell\ell})_{1111} \sim (g_{\mathcal{W}}^{\ell})^2$ and the aforementioned reason in case of $g_{\mathcal{W}}^{\varphi}$. In fact, these bounds can be considered meaningless since they are of the order or above the perturbative limit 4π and well in excess of more refined perturbative unitarity bounds [43]. The four-heavy operators $c_{QQ}^{(1,8)}$ are responsible for the increased sensitivity we observe in $(g_{\mathcal{W}}^g)_{33}$ after including quadratic EFT corrections.

Finally, concerning the models \mathcal{G} , \mathcal{H} , \mathcal{Q}_5 and \mathcal{Y}_5 , we observe a significant tightening of the bounds after quadratic EFT corrections are accounted for. This is entirely due to their sensitivity to the four-heavy operators, as can be seen in Table 4.2.

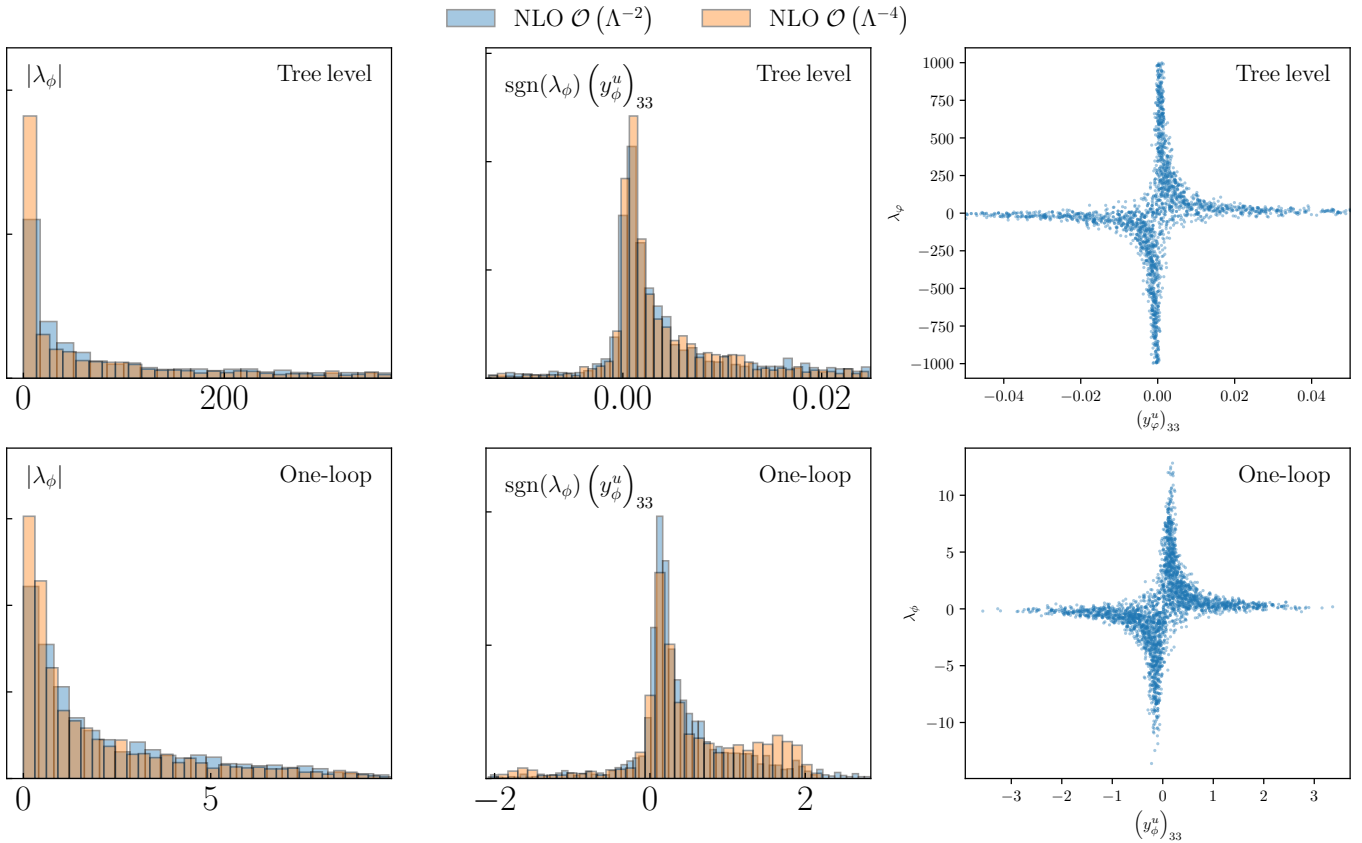


Figure 4.3: Marginalized posterior distributions of the two UV invariants associated to the heavy scalar model ϕ , comparing the impact of linear and quadratic EFT corrections after matching at tree level (upper panel) and at one-loop level (lower panel). The rightmost panels illustrate how the individual UV couplings λ_ϕ and $(y_\phi^u)_{33}$ are correlated, as expected given that only their product can be constrained from the data. See Table 4.5 for the corresponding 95% CL intervals.

Comparison to the FITMAKER results. The global SMEFT analysis carried out in [16] by the FITMAKER collaboration also provided bounds for selected single-particle extensions of the SM obtained from tree-level matching. Specifically, they provide results for 21 different models including heavy scalars, fermions, and vector bosons. These UV models were highlighted in red in Tables 4.2 and 4.3.

As further discussed in App. D, the FITMAKER models are assumed to couple in a flavour-universal way to the SM fields. This flavour assumption is inconsistent with the corresponding one adopted by SMEFT and leads in most models to the generation of non-vanishing EFT coefficients which are not part of our baseline fitting basis. Furthermore, in some scenarios, like in the heavy scalar ϕ model, they lead to coefficients with flavour indices breaking the SMEFT flavour symmetries. For this reason, in order to benchmark our results for the single-particle BSM extensions with those of [16], we adopt their same matching relations and ignore the effects of EFT coefficients not included in our fit.

We provide in Fig. 4.6 a comparison between the upper 95% CL bounds on the absolute value of the UV couplings g_{UV} for the single-particle extensions obtained in [16] with the results of this work, where a heavy particle mass of $m_{UV} = 1$ TeV is assumed for all models. We find satisfactory agreement for most of the models considered, with residual differences between the FITMAKER bounds (based on a linear EFT fit at LO) and our own ones with the same theory settings explained by different choices of the input dataset and of their statistical treatment.

Non-negligible differences are instead observed for the heavy scalar model ϕ , the heavy fermion model Q_{17} , and the heavy vector models \mathcal{W}_1 and $\mathcal{B}_1\mathcal{B}$. Differences for the ϕ model are explained by the fact that the SMEFT basis includes four-heavy operators generated by this model, such as c_{Qt}^1 and c_{Qt}^8 (Table 4.2), constrained by $t\bar{t}b\bar{b}$ and $t\bar{t}t\bar{t}$ cross-sections and which are absent from the FITMAKER analysis. Differences

■ NLO $\mathcal{O}(\Lambda^{-2})$ ■ NLO $\mathcal{O}(\Lambda^{-4})$

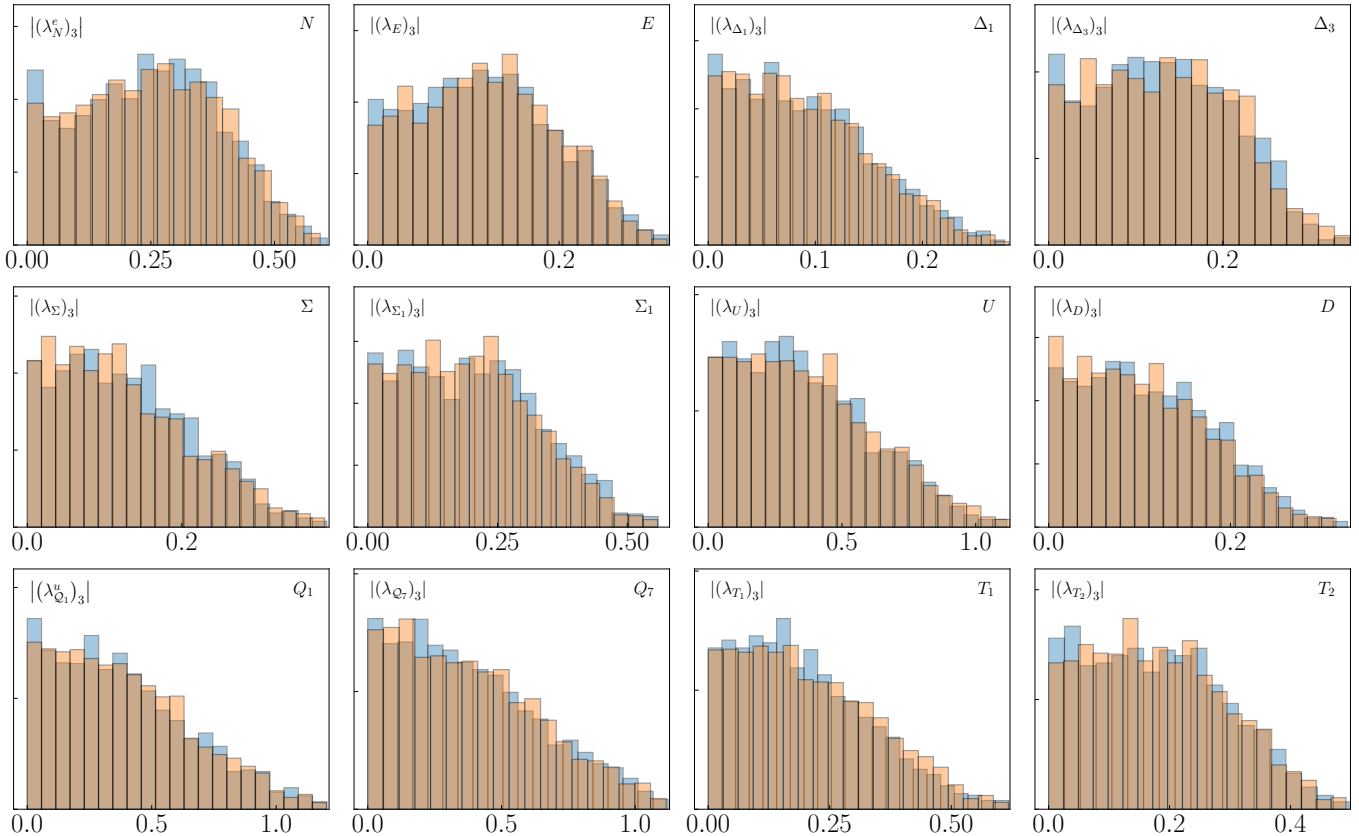


Figure 4.4: Same as Fig. 4.1 for the one-particle models composed of heavy vector-like fermions

for the fermionic model Q_{17} as well as for the heavy vector models \mathcal{W}_1 and $\mathcal{B}_1\mathcal{B}$ originate from the inclusion of different Higgs production datasets in the fit.

From the comparison in Fig. 4.6, one further observes that the change in sensitivity after including either NLO QCD or quadratic EFT corrections is mild, indicating that for these models the dominant sensitivity on the UV couplings is already provided by the linear EFT predictions with LO accuracy. In this context, one should note that a 20% improvement at the level of the Wilson coefficients c_i corresponds to only a 10% enhancement at the level of the UV parameters g_{UV} given that the typical matching relations have the form $c_i \sim g_{UV}^2$.

All in all, we conclude that this comparison with FITMAKER is successful and provides a non-trivial validation of our new pipeline enabling direct fits of UV couplings within the SMEFIT framework.

4.2 Multi-particle models matched at tree level

Moving beyond one-particle models, we now study UV-completions of the SM which include multiple heavy particles. Specifically, we consider a UV model which includes two heavy vector-like fermions, Q_1 and Q_7 , and a heavy vector-boson, \mathcal{W} , see Table 4.1 for their quantum numbers and gauge group representation. In the case of equal masses and couplings for the two heavy fermions, this model satisfies custodial symmetry [40]. The two heavy fermions Q_1 and Q_7 generate the same two operators, namely $c_{t\varphi}$ and $c_{\varphi t}$. A contribution to the top Yukawa operator $c_{t\varphi}$ is also generated by the heavy vector-boson \mathcal{W} , introducing an interesting interplay between the quark bidoublets on the one hand and the neutral vector triplet on the other hand. As indicated in Table 4.2, several other operators in addition to $c_{t\varphi}$ are generated when integrating out the heavy vector boson \mathcal{W} .

It should be emphasized that we make this choice of multi-particle model for illustrative purposes as well as to compare with the benchmark studies of [40], and that results for any other combination of the

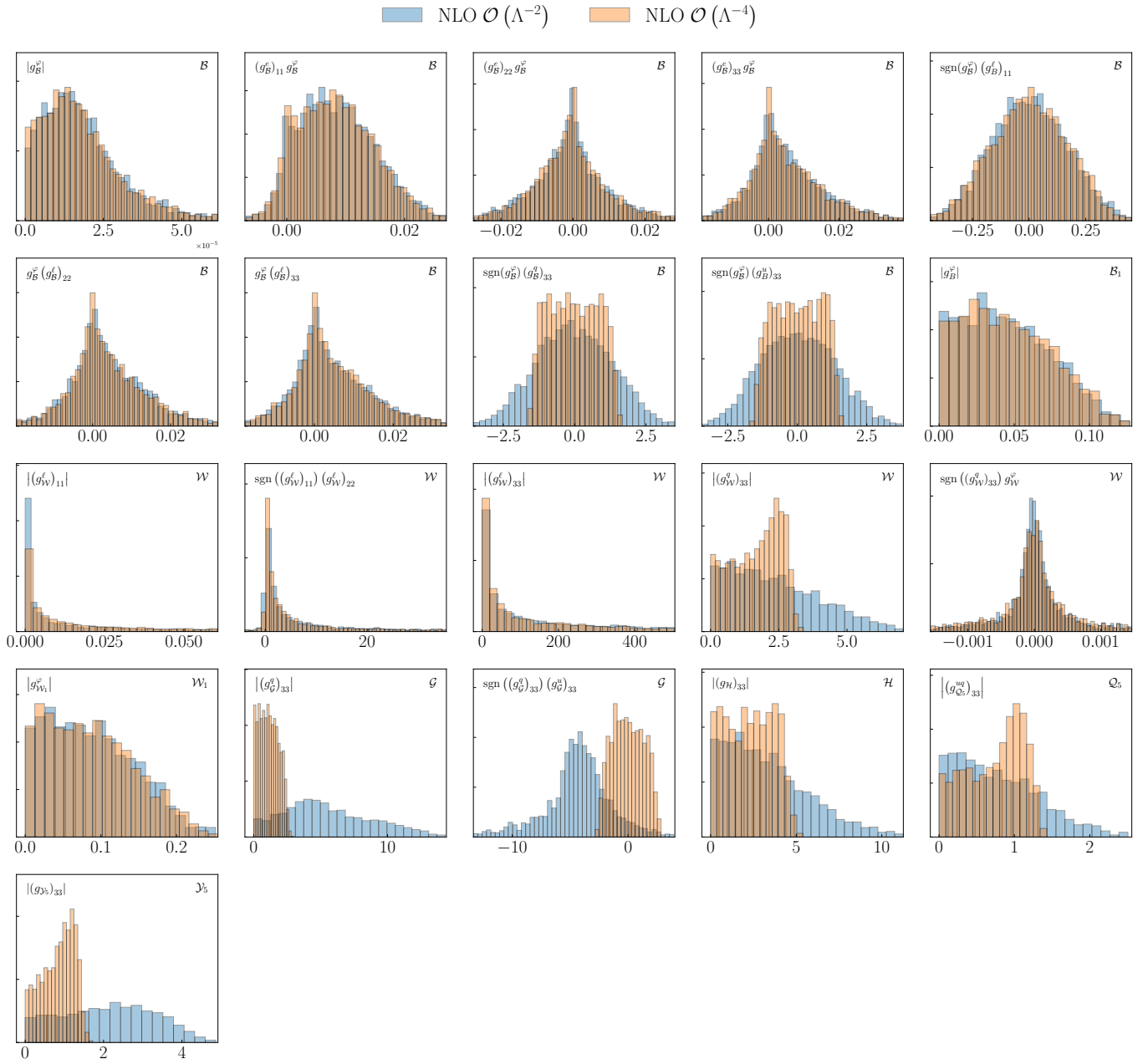


Figure 4.5: Same as Fig. 4.1 for the one-particle models composed of heavy vector-like bosons

heavy BSM particles listed in Table 4.1 can easily be obtained within our approach. The only limitations are that the number of UV couplings must remain smaller than the number of EFT coefficients entering the analysis, and that the input data used in the global fit exhibits sensitivity to the matched UV model.

We provide in Table 4.7 the 95% CL intervals for the UV invariants associated to this three-particle model. A common value of the heavy mass, $m_{Q_1} = m_{Q_7} = m_W = 1$ TeV, is assumed. As in the case of the one-particle models, we compare results at the linear and quadratic EFT level and at LO and NLO in the QCD expansion. The associated posterior distributions for the UV invariants comparing the impact of linear versus quadratic EFT corrections are shown in Fig. 4.7. On the one hand, one notices an increase in sensitivity at the quadratic level in case of $(g_{WV}^q)_{33}$, which is consistent with the results of the one-particle model analysis shown in Table 4.6. On the other hand, for some of the UV-invariants in the model, such as $|(g_{WV}^l)_{11}|$, the bounds become looser once quadratic EFT corrections are accounted for, presumably due to the appearance of a second minimum in the marginalised χ^2 profiles. For this specific model, it turns out that one has a quasi-flat direction in the UV-invariant $|(g_{WV}^l)_{33}|$.

While the results of Table 4.6 assume a common value of the heavy particle masses, it is trivial to

Model	UV invariants	LO $\mathcal{O}(\Lambda^{-2})$	LO $\mathcal{O}(\Lambda^{-4})$	NLO $\mathcal{O}(\Lambda^{-2})$	NLO $\mathcal{O}(\Lambda^{-4})$
\mathcal{B}	$ g_{\mathcal{B}}^{\varphi} $	$[0, 4.4 \cdot 10^{-5}]$	$[0, 4.4 \cdot 10^{-5}]$	$[0, 4.6 \cdot 10^{-5}]$	$[0, 4.6 \cdot 10^{-5}]$
	$(g_{\mathcal{B}}^e)_{11} g_{\mathcal{B}}^{\varphi}$	$[-0.0033, 0.021]$	$[-0.0028, 0.021]$	$[-0.0022, 0.022]$	$[-0.0032, 0.021]$
	$(g_{\mathcal{B}}^e)_{22} g_{\mathcal{B}}^{\varphi}$	$[-0.026, 0.022]$	$[-0.026, 0.022]$	$[-0.025, 0.025]$	$[-0.025, 0.025]$
	$(g_{\mathcal{B}}^e)_{33} g_{\mathcal{B}}^{\varphi}$	$[-0.015, 0.030]$	$[-0.015, 0.029]$	$[-0.016, 0.029]$	$[-0.014, 0.030]$
	$\text{sgn}(g_{\mathcal{B}}^{\varphi}) (g_{\mathcal{B}}^e)_{11}$	$[-0.32, 0.33]$	$[-0.33, 0.32]$	$[-0.32, 0.33]$	$[-0.32, 0.30]$
	$g_{\mathcal{B}}^{\varphi} (g_{\mathcal{B}}^e)_{22}$	$[-0.016, 0.027]$	$[-0.016, 0.027]$	$[-0.016, 0.028]$	$[-0.016, 0.029]$
	$g_{\mathcal{B}}^{\varphi} (g_{\mathcal{B}}^e)_{33}$	$[-0.014, 0.028]$	$[-0.015, 0.027]$	$[-0.014, 0.029]$	$[-0.015, 0.028]$
	$\text{sgn}(g_{\mathcal{B}}^{\varphi}) (g_{\mathcal{B}}^q)_{33}$	$[-3.1, 3.0]$	$[-1.4, 1.5]$	$[-2.4, 2.6]$	$[-1.4, 1.4]$
$\text{sgn}(g_{\mathcal{B}}^{\varphi}) (g_{\mathcal{B}}^u)_{33}$	$[-3.2, 2.9]$	$[-1.5, 1.4]$	$[-2.5, 2.6]$	$[-1.4, 1.4]$	
\mathcal{B}_1	$ g_{\mathcal{B}}^{\varphi} $	$[0, 0.099]$	$[0, 0.098]$	$[0, 0.098]$	$[0, 0.099]$
\mathcal{W}	$ g_{\mathcal{W}}^e)_{11} $	$[0, 0.33]$	$[0, 0.32]$	$[0, 0.28]$	$[0, 0.34]$
	$\text{sgn}((g_{\mathcal{W}}^e)_{11}) (g_{\mathcal{W}}^e)_{22}$	$[-34, 4.6 \cdot 10^2]$	$[-20, 5.3 \cdot 10^2]$	$[-17, 7.0 \cdot 10^2]$	$[-21, 3.6 \cdot 10^1]$
	$ g_{\mathcal{W}}^e)_{33} $	$[0, 7.9 \cdot 10^2]$	$[0, 7.8 \cdot 10^2]$	$[0, 8.0 \cdot 10^2]$	$[0, 7.7 \cdot 10^2]$
	$ g_{\mathcal{W}}^q)_{33} $	$[0, 6.4]$	$[0, 3.1]$	$[0, 5.6]$	$[0, 2.9]$
	$\text{sgn}((g_{\mathcal{W}}^q)_{33}) g_{\mathcal{W}}^{\varphi}$	$[-0.022, 0.019]$	$[-0.024, 0.017]$	$[-0.026, 0.020]$	$[-0.024, 0.020]$
\mathcal{G}	$ g_{\mathcal{G}}^q)_{33} $	$[0, 12]$	$[0, 2.5]$	$[0, 12]$	$[0, 2.3]$
	$\text{sgn}((g_{\mathcal{G}}^q)_{33}) (g_{\mathcal{G}}^u)_{33}$	$[-11, 1.8]$	$[-2.3, 2.6]$	$[-11, 2.2]$	$[-2.2, 2.4]$
\mathcal{H}	$ g_{\mathcal{H}})_{33} $	$[0, 8.0]$	$[0, 4.3]$	$[0, 8.0]$	$[0, 4.4]$
\mathcal{Q}_5	$ g_{\mathcal{Q}_5}^{uq})_{33} $	$[0, 2.1]$	$[0.026, 1.4]$	$[0, 1.8]$	$[0, 1.3]$
\mathcal{Y}_5	$ g_{\mathcal{Y}_5})_{33} $	$[0.046, 4.5]$	$[0.031, 1.6]$	$[0, 4.0]$	$[0.053, 1.4]$

Table 4.6: Same as Table 4.4 for the UV invariants associated to the one-particle heavy vector boson extensions

Model	UV invariants	LO $\mathcal{O}(\Lambda^{-2})$	LO $\mathcal{O}(\Lambda^{-4})$	NLO $\mathcal{O}(\Lambda^{-2})$	NLO $\mathcal{O}(\Lambda^{-4})$
(Q_1, Q_7, \mathcal{W})	$ g_{\mathcal{W}}^l)_{11} $	$[0, 0.43]$	$[0, 0.31]$	$[0, 0.36]$	$[0, 0.28]$
	$\text{sgn}((g_{\mathcal{W}}^l)_{11}) (g_{\mathcal{W}}^l)_{22}$	$[-3.3, 40]$	$[-3.9, 49]$	$[-4.7, 53]$	$[-4.8, 49]$
	$ g_{\mathcal{W}}^l)_{33} $	$[0, 7.7 \cdot 10^2]$	$[0, 7.9 \cdot 10^2]$	$[0, 7.4 \cdot 10^2]$	$[0, 7.6 \cdot 10^2]$
	$ g_{\mathcal{W}}^q)_{33} $	$[0, 6.5]$	$[0.011, 3.1]$	$[0, 5.4]$	$[0.014, 2.9]$
	$\text{sgn}((g_{\mathcal{W}}^q)_{33}) g_{\mathcal{W}}^{\varphi}$	$[-0.013, 0.012]$	$[-0.014, 0.019]$	$[-0.013, 0.0099]$	$[-0.014, 0.011]$
	$ (\lambda_{\mathcal{Q}_1}^u)_3 $	$[0, 0.87]$	$[0, 0.88]$	$[0, 0.86]$	$[0, 0.86]$
	$ (\lambda_{\mathcal{Q}_7})_{33} $	$[0, 0.88]$	$[0, 0.87]$	$[0, 0.84]$	$[0, 0.87]$

Table 4.7: Same as Table 4.4 for the UV invariants associated to the three-particle model consisting of two heavy fermions Q_1, Q_7 and a heavy vector boson \mathcal{W} obtained from tree-level matching. A common value of the heavy mass is assumed for the three particles, $m_{Q_1} = m_{Q_7} = m_{\mathcal{W}} = 1$ TeV. See Fig. 4.8 for the corresponding results in a scenario with $m_{Q_1} \neq m_{Q_7} \neq m_{\mathcal{W}}$. For this model we have a flat direction in the UV-invariant $|g_{\mathcal{W}}^l)_{33}|$.

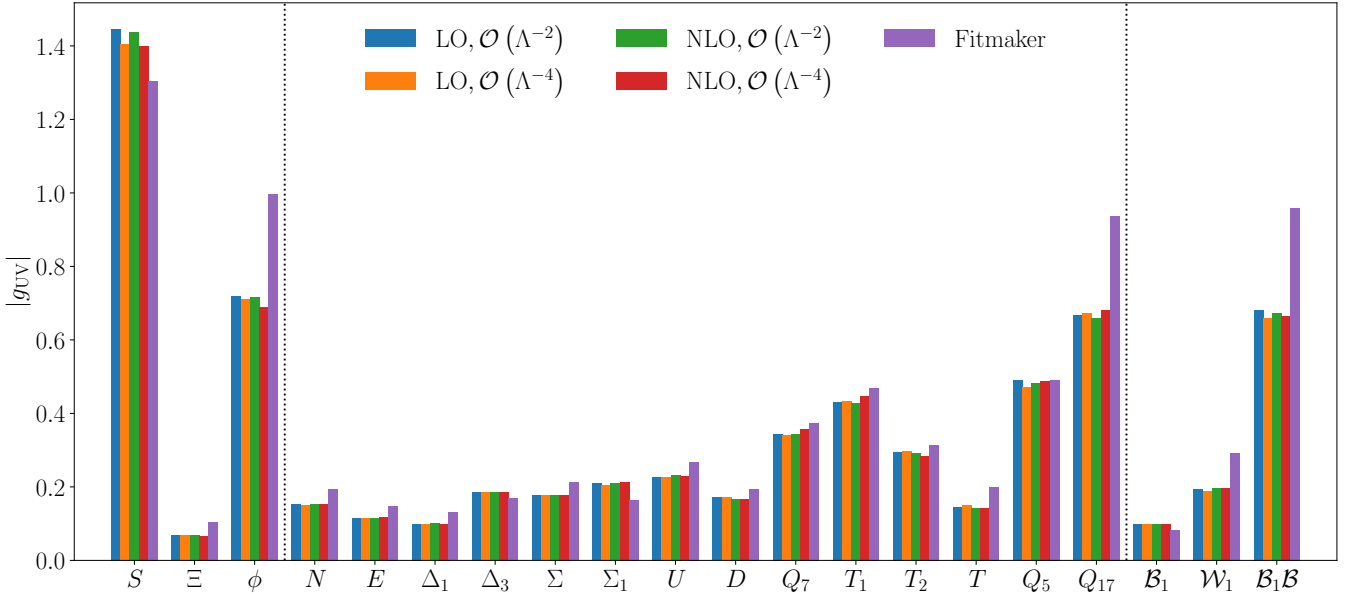


Figure 4.6: Upper 95% CL bounds on the absolute value of the UV couplings g_{UV} obtained for the single-particle extensions considered in [16] compared to the results of this work. A heavy particle mass of $m_{UV} = 1$ TeV is assumed. We display sequentially the results for the scalar, fermion, and vector particles separated by vertically dashed lines.

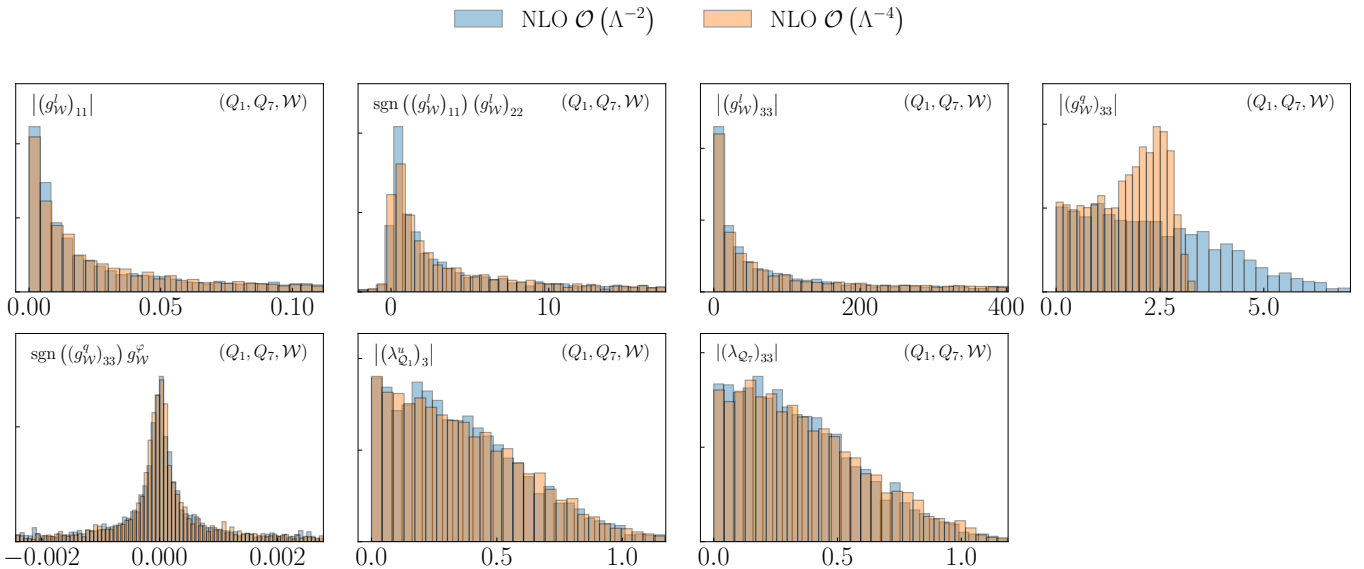


Figure 4.7: The posterior distributions of the UV invariants in the three-particle model consisting of two heavy fermions Q_1, Q_7 and a heavy vector boson \mathcal{W} , see also see Table 4.7, comparing the impact of linear (blue) versus quadratic (orange) corrections in the EFT expansion.

extend them to different masses for each of the different particles in the model. This way, one can assess the dependence of the UV-coupling fit results on the assumptions of the heavy particle masses. With this motivation, Fig. 4.8 and Fig. 4.9 display pair-wise marginalised 95% contours for the relevant UV invariants and the original Lagrangian parameters in the model respectively, see Fig. 4.7 for the corresponding single-invariant posterior distributions. The baseline results with a common mass of 1 TeV are compared to a scenario with three different heavy masses, $m_{Q_1} = 3$ TeV, $m_{Q_7} = 4.5$ TeV, and $m_{\mathcal{W}} = 2.5$ TeV. We exclude $|(g_W^l)_{33}|$ from this comparison, given that it is essentially unconstrained from the fitted data.

From the comparison in Fig. 4.8 one observes, as expected, that assuming heavier BSM particles leads to looser constraints on the UV couplings. Taking into account that different terms in the matching

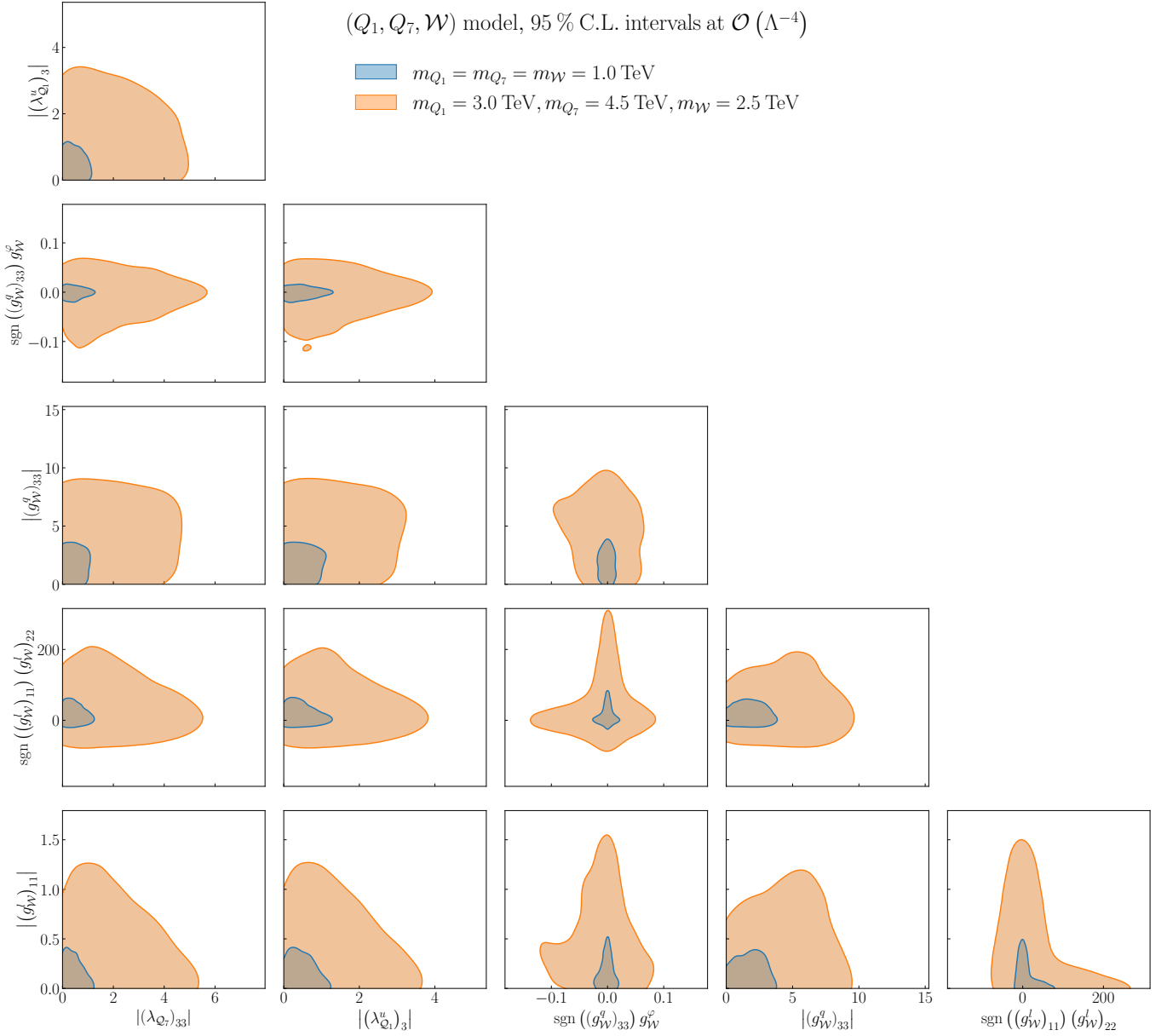


Figure 4.8: Pair-wise marginalised 95% contours for the UV invariants associated to the three-particle model consisting of two heavy fermions, Q_1 and Q_7 , and the heavy vector boson \mathcal{W} , see also Fig. 4.7 and Table 4.7 for the corresponding single-invariant posterior distributions and 95% CL bounds. We compare results for a common value of the heavy mass, $m_{Q_1} = m_{Q_7} = m_{\mathcal{W}} = 1 \text{ TeV}$, with another scenario with different heavy masses, $m_{Q_1} = 3 \text{ TeV}$, $m_{Q_7} = 4.5 \text{ TeV}$, and $m_{\mathcal{W}} = 2.5 \text{ TeV}$. The EFT fit is carried out at NLO QCD with $\mathcal{O}(\Lambda^{-4})$ corrections included. As compared to the list of invariants in Table 4.7, we exclude $|(g_{\mathcal{W}}^t)_{33}|$ given that it is essentially unconstrained from the fitted data.

relations scale with the heavy particle masses in a different manner, it is not possible in general to rescale the bounds obtained from the equal mass scenario to another with different heavy masses. Nevertheless, given that in a single-particle extension we know that bounds worsen by a factor $(m_{\text{UV}}^*/m_{\text{UV}})^2$ if the heavy particle mass is increased from m_{UV} up to m_{UV}^* , one can expect that in this three-particle scenario the bounds are degraded by an amount between ~ 5 and ~ 20 depending on the specific UV coupling, a estimate which is consistent with the results in Fig. 4.8. This comparison also highlights how for very heavy particles we lose all sensitivity and the global EFT fit cannot provide competitive constraints on the UV model parameters.

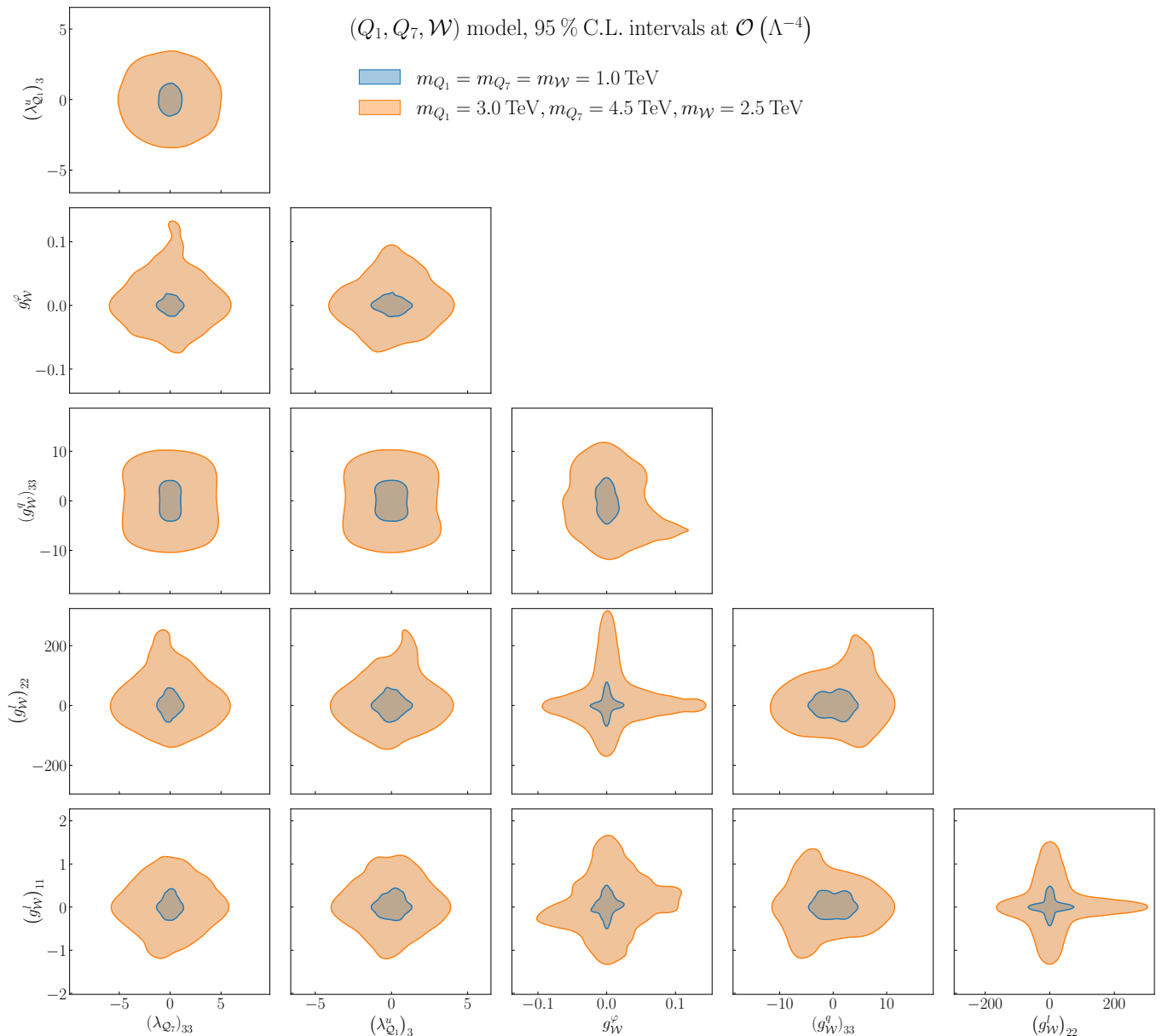


Figure 4.9: Same as Fig. 4.8 in the case of the original UV couplings.

4.3 Single-particle models matched at one-loop

All results presented so far relied on tree-level matching relations. We now present results for UV-coupling fits in the case of matching relations obtained at the one-loop level, and study their effect on the UV parameter space as compared to results based on tree-level matching. As discussed in Sect. 2.2, for this purpose we can also deploy `MATCHMAKEREFT` interfaced to `SMEFIT` via `MATCH2FIT` in order to obtain one-loop matching relations suitable for their use in the fit in an automated way². In its current incarnation, this pipeline enables using any of the single-particle heavy scalar and heavy fermion models (and combinations thereof) listed in Table 4.1 when matched at the one-loop level. We note here that the automation of the one-loop matching for heavy vector bosons has not been achieved yet. For concreteness, here we present results based on the one-loop matching the heavy scalar ϕ defined by Eq. (2.1), and also discussed in Sect. 4.1, in order to compare its bounds to those previously obtained from the tree-level matching analysis.

Table 4.5 compares the 95% CL bounds obtained for the two UV invariants in this model following either tree-level or one-loop matching relations, with the associated marginalised posterior distributions

²A development version of `MATCH2FIT` suitable to one-loop matching relations can be obtained upon request.

shown in Fig. 4.3. In contrast to the bounds obtained at tree-level, one-loop corrections enable lifting the flat direction along the $|\lambda_\phi|$ invariant. This effect is a consequence of the operators $\mathcal{O}_{\varphi\Box}$, $\mathcal{O}_{b\varphi}$ and $\mathcal{O}_{t\varphi}$, which receive additional one-loop matching contributions resulting in independent constraints on λ_ϕ . Specifically, the one-loop matching relations for the Wilson coefficients associated to $\mathcal{O}_{\varphi\Box}$ and $\mathcal{O}_{t\varphi}$ read

$$\begin{aligned}\frac{c_{\varphi\Box}}{\Lambda^2} &= -\frac{g_1^4}{7680\pi^2} \frac{1}{m_\phi^2} - \frac{g_2^4}{2560\pi^2} \frac{1}{m_\phi^2} - \frac{3}{32\pi^2} \frac{\lambda_\phi^2}{m_\phi^2}, \\ \frac{c_{t\varphi}}{\Lambda^2} &= -\frac{\lambda_\phi (y_\phi^u)_{33}}{m_\phi^2} - \frac{g_2^4 y_t^{\text{SM}}}{3840\pi^2} \frac{1}{m_\phi^2} + \frac{y_t^{\text{SM}}}{16\pi^2} \frac{\lambda_\phi^2}{m_\phi^2} + \frac{(4(y_b^{\text{SM}})^2 - 13(y_t^{\text{SM}})^2)}{64\pi^2} \frac{\lambda_\phi (y_\phi^u)_{33}}{m_\phi^2} \\ &\quad - \left(12\lambda_\phi^{\text{SM}} + (y_b^{\text{SM}})^2 - 11(y_t^{\text{SM}})^2\right) \frac{y_t^{\text{SM}}}{64\pi^2} \frac{(y_\phi^u)_{33}^2}{m_\phi^2} + \frac{3}{128\pi^2} \frac{\lambda_\phi (y_\phi^u)_{33}^3}{m_\phi^2},\end{aligned}\tag{4.4}$$

where λ_ϕ^{SM} is the quartic Higgs self-coupling in the SM. In Eq. (4.4), all terms with a factor $1/\pi^2$ arise from one-loop corrections, indicating that $c_{\varphi\Box}$ is entirely loop-generated while for $c_{t\varphi}$ the tree-level matching relation is simply $c_{t\varphi} = -\lambda_\phi (y_\phi^u)_{33}/m_\phi^2$. This additional dependence on λ_ϕ arising from one-loop corrections is hence responsible for closing the tree-level flat direction. We have also checked that the bounds resulting from one-parameter SMEFT fits of the Wilson coefficients $c_{\varphi\Box}$ and $c_{t\varphi}$ to the same datasets lead to similar bounds on $|\lambda_\phi|$ as compared to those reported in Table 2.1 after using the relations in Eq. (4.4)

On the other hand, as a consequence of one-loop corrections to the matching relations one also observes a degradation in the sensitivity to the UV-invariant $\text{sgn}(\lambda_\phi)(y_\phi^u)_{33}$. The reason is that the parameter region around arbitrarily small values of the coupling $(y_\phi^u)_{33}$ is disfavoured now, translating into a flattening of the distribution in $(y_\phi^u)_{33}$ as observed in the rightmost panels of Fig. 4.3. These results showcase that one-loop corrections bring in not only precision but also accuracy, in that the stronger bound on this UV-invariant at tree-level was a consequence of a flat direction which is lifted as soon as perturbative corrections are accounted for.

Interestingly, the middle panels of Fig. 4.3 also indicate the appearance of a double-peak structure in the distribution of $\text{sgn}(\lambda_\phi)(y_\phi^u)_{33}$ at quadratic order in the EFT expansion which is absent in case of tree-level matching. Such structure is associated to a second minimum in the χ^2 favouring non-zero UV couplings, and may be related to cancellations between different terms in the matching relations.³ For one-loop matching relations such as those displayed in Fig. 4.4, the minimised figure of merit will in general be a complicated higher-order polynomial in the UV couplings, and in particular in the presence of quadratic EFT corrections, the $\chi^2(\mathbf{c})$ will be a quartic form of the Wilson coefficients. Therefore, for the specific case of the heavy scalar model, the $\chi^2(\mathbf{g})$ expressed in terms of the UV couplings will include terms of up to $\mathcal{O}(\lambda_\phi^8)$ and $\mathcal{O}((y_\phi^u)_{33}^{16})$, see Eqns (4.4) and (2.11), as well as the various cross-terms. The minima structure of $\chi^2(\mathbf{g})$ can then only be resolved by means of a numerical analysis such as the one enabled by our strategy.

The above discussion demonstrates that one-loop corrections to the SMEFT matching relations provide non-trivial information on the parameter space of the considered UV models. Loop corrections not only modify the sensitivity to UV couplings already constrained by tree-level, but can also lift flat or quasi-flat directions. This result further motivates ongoing efforts to increase the perturbative accuracy of EFT matching relations.

5 Summary and outlook

In this work we have presented and validated a general strategy to scrutinize the parameters of BSM models by using the SMEFT as an intermediate bridge to the experimental data. By combining MATCHMAKEREFT

³Such cancellations may arise in EFT fits whenever linear and quadratic corrections become comparable.

(for the matching between UV models and the EFT) with `MATCH2FIT` (for the conversion of the matching results to fit run card) and `SMEFIT` (for the comparison with data and derivation of posterior distributions), this pipeline enables to constrain the masses and couplings of any UV model that can be matched to the SMEFT either at tree-level or at one-loop. While in this work we adopt `MATCHMAKEREFT`, our approach is fully general and any other matching framework could be adopted.

This flexible pipeline results in the automation of the bound-setting procedure on UV-complete models that can be matched to the SMEFT. To illustrate its reach, we apply it to derive constraints on a wide range of single-particle models extending the SM with heavy scalars, fermions, or vector bosons with different quantum numbers. We also consider a three-particle model which combines two heavy vector-like fermions with a vector boson. While most of the results presented arise from tree-level matching relations, we also demonstrate how our approach can be used in the case of one-loop matching using the heavy scalar model as a proof-of-concept.

All the tools used in this analysis are made publicly available, ensuring the reproducibility of our results and enabling their extension to analyse other user-defined BSM scenarios. In addition to a new version of `SMEFIT` with the option of performing fits in the parameter space of UV couplings, we release the Mathematica package `MATCH2FIT` whose goal is to streamline the interface between EFT matching and fitting codes. In its current incarnation, `MATCH2FIT` connects `MATCHMAKEREFT` with `SMEFIT`, but could be extended to other combinations in the future. The availability of this pipeline opens up therefore the possibility of easily including SMEFT-derived constraints in upcoming model-building efforts.

There are several directions that could be considered for future work generalising the results presented in this work. The most obvious one would be achieving the full automation of one-loop matching relations entering the global EFT fit, including the evaluation of the associated UV invariants, for multi-particle models. One restriction here is that one-loop matching is not yet automated for models including heavy vector bosons. As we have shown in the case of the heavy scalar model, one-loop matching relations make it possible to derive new constraints on parameter directions which are flat after tree-level matching, resolving degeneracies both among models and in the space of UV couplings.

Furthermore, including dimension-8 operators in the fit, which are also generated by the matching relations, could help to disentangle models via the evaluation of their positivity bounds [34]. While a bottom-up determination of dimension-8 operators from data is hampered by their large number in the absence of extra assumptions, specific UV models only generate a relatively small number of dimension-8 operators, facilitating their integration in the SMEFT fit. One could also consider accounting for RGE effects between the cutoff scale given by the UV model and the scale at which the global fit is performed. The latter could be combined with the inclusion of RGE effects in the cross sections entering the fit [32]. Finally, it would be beneficial to consider more flexible flavour symmetries which are automatically consistent with the fitting code, something which would anyway be required for a full extension of multi-particle models to one-loop matching.

All in all, our results provide valuable insights on ongoing model-building efforts by using the SMEFT to connect them with the experimental data, hence providing complementary information to that derived from direct searches for new heavy particles at the LHC and elsewhere. The pipeline presented in this work brings closer one of the original goals of the EFT program at the LHC, namely bypassing the need to directly compare the predictions of UV-complete models with the experimental measurements and instead using the SMEFT as the bridge connecting UV physics with data.

Acknowledgments

We acknowledge useful discussions with J. Santiago, M. Chala, K. Mimasu, C. Severi, F. Maltoni, L. Mantani, T. Giani, J. Pagès, A. Thomsen, and Y. Oda. A. R. thanks the High Energy Theory Group of Universidad de Granada and Theory Group of Nikhef for their hospitality during early stages of this work. The work of A. R. and E. V. is supported by the European Research Council (ERC) under the European

Union’s Horizon 2020 research and innovation programme (Grant agreement No. 949451) and by a Royal Society University Research Fellowship through grant URF/R1/201553. The work of J. t. H. and G. M is supported by the Dutch Research Council (NWO). The work of J. R. is supported by the Dutch Research Council (NWO) and by the Netherlands eScience Center.

A Baseline SMEFiT global analysis

The SMEFiT framework provides a flexible and robust open-source tool to constrain the SMEFT parameter space using the information provided by experimental data from energy-frontier particle colliders such as the LHC as well as from lower-energy experiments.

Given a statistical model defined by a likelihood $L(\mathbf{c})$, depending on parameters \mathbf{c} specifying the theoretical predictions for the observables entering the fit, and the corresponding dataset \mathcal{D} , SMEFiT infers the posterior distribution $P(\mathbf{c}|\mathcal{D})$ by means of sampling techniques [44, 45]. SMEFiT supports the inclusion of quadratic EFT corrections, can work up to NLO precision in the QCD expansion, admits general user-defined flavour assumptions and theoretical restrictions, and does not have limitations on the number or type of dimension-six operators that can be considered.

Theoretical restrictions on the EFT parameter space can be imposed as follows. Given a set of N fit coefficients $\{c_1, \dots, c_N\}$, SMEFiT allows the user to impose relations of the general form,

$$\sum_i a_i (c_1)^{n_{1,i}} \dots (c_N)^{n_{N,i}} = 0, \quad (\text{A.1})$$

where the sum runs over all the possible combinations of the coefficients and $n_{j,i}$ are real numbers such that $\sum_j n_{j,i}$ is equal to a constant to preserve the correct dimensionality for all i . For instance, the relationship between the Wilson coefficients in Eq. (2.4) arising from the heavy scalar model matched at tree-level can be rewritten in the same format as Eq. (A.1), namely

$$\left(c_{qd}^{(1)}\right)_{3333} \left((c_{u\varphi})_{33}\right)^2 - \left(c_{qu}^{(1)}\right)_{3333} \left((c_{d\varphi})_{33}\right)^2 = 0 \quad (\text{A.2})$$

These relations have to be imposed on a case-by-case basis via a run card and the user must declare which are the independent coefficients to be fitted. This functionality can be used to either relate the fit parameters among them, as in Eq. (A.2), or to perform a mapping to a different set of degrees of freedom. The latter feature allows one to perform with SMEFiT the fits on the UV model parameters as presented in this work.

As mentioned in Sect. 3, in comparison to [23], which in turn updates the global SMEFT analysis of Higgs, top quark, and diboson data presented in [22], here we implement in SMEFiT the information provided by the legacy electroweak precision observables (EWPOs) from LEP and SLAC [35] in an exact manner. Previously, the constraints provided by these EWPOs in the SMEFT parameter space were accounted in an approximate manner, assuming EWPOs were measured with vanishing uncertainties. This assumption introduced additional relations between a subset of the Wilson coefficients. While such approximation served the purposes of interpreting LHC measurements, it is not appropriate in the context of matching to UV-complete models given that in many BSM scenarios the EWPOs provide the dominant constraints [16]. The new implementation of EWPOs in SMEFiT will be discussed in a separate publication [39] and here we provide for completeness a short summary.

Experimental data and SM predictions for the legacy EWPOs from LEP and SLAC are taken from [35]. Linear and quadratic SMEFT corrections to these observables arising from dimension-six operators have been computed with MG5_AMC@NLO interfaced to SMEFT@NLO. Our implementation of the EWPOs has been benchmarked by comparing with the results of [46], assuming the same theoretical settings and choice of input dataset. Specifically, for this benchmarking exercise we use the m_W electroweak input scheme, linear EFT corrections, LO cross-sections, and assume flavour universality. Furthermore, we adopt the same convention on triple gauge operator O_{WWW} , which differs from SMEFT@NLO by a negative sign.

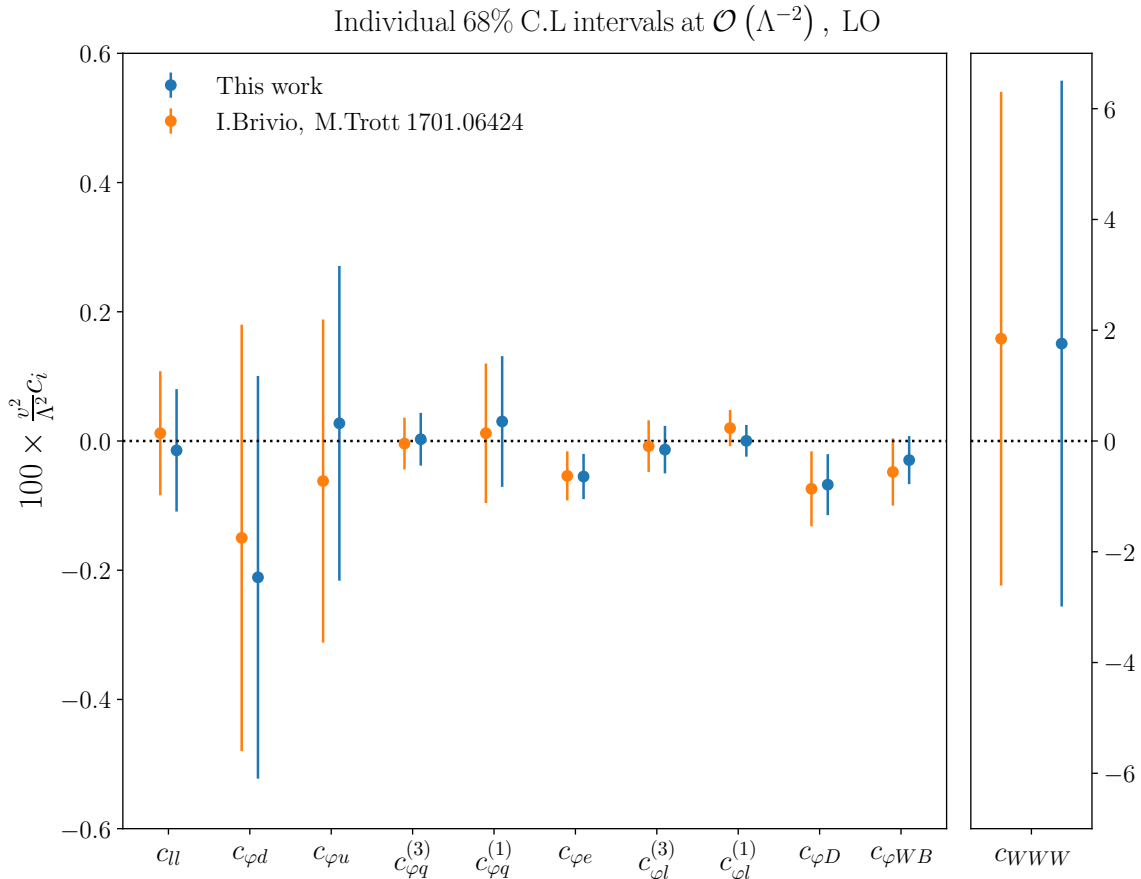


Figure A.1: Comparison of a SMEFT-based analysis of the electroweak precision observables from LEP against the corresponding analysis from [46] based on the same dataset. We display bounds at the 68% CL for one-parameter fits using linear EFT and LO calculations. In this comparison, we adopt the convention of [46] for the triple gauge operator O_{WWW} , which differs from the SMEFT@NLO one by a negative sign. For consistency with the settings adopted in [46], the triple gauge operator c_{WWW} has been fitted to a subset of the available LEP data composed by only 4 bins.

Fig. A.1 displays the bounds at the 68% CL for one-parameter fits in the two studies. Good agreement between our implementation and that of [46] is obtained for all operators. Residual differences can be explained due to the inclusion of flavour-sensitive observables from LEP which are absent in [46].

Taking into account this updated EWPOs implementation, when compared to the results of [22, 23] the present global SMEFT analysis used to constrain UV models contains 14 additional Wilson coefficients \mathbf{c} to be constrained from the fit for a total of 50 independent parameters. The new degrees of freedom are constrained not only by the EWPOs, but also top quark and diboson measurements. For this reason, we have recomputed EFT cross-sections for all the processes where such operators are relevant. As in the original analysis [22], we use MG5_AMC@NLO interfaced to SMEFT@NLO to evaluate linear and quadratic EFT corrections which are augmented with NLO QCD perturbative corrections whenever available. To avoid overlap between datasets entering the PDF and EFT fits [47, 48], we use NNPDF4.0 NNLO no-top [49] as input PDF set. The values of the input electroweak parameters are taken to be $m_W = 80.387$ GeV, $m_Z = 91.1876$ GeV and $G_F = 1.1663787 \cdot 10^{-5}$ GeV⁻². Finally, the same flavour assumptions as in [22] are used i.e. a $U(2)_q \times U(2)_u \times U(3)_d \times [U(1)_\ell \times U(1)_e]^3$ symmetry in the quark and lepton sectors.

In addition to Fig. 3.2, the impact of the exact implementation of EWPOs in the SMEFT fit is also illustrated in Fig. A.2, which compares the 68% and 95% CL marginalised bounds on the Wilson coefficients

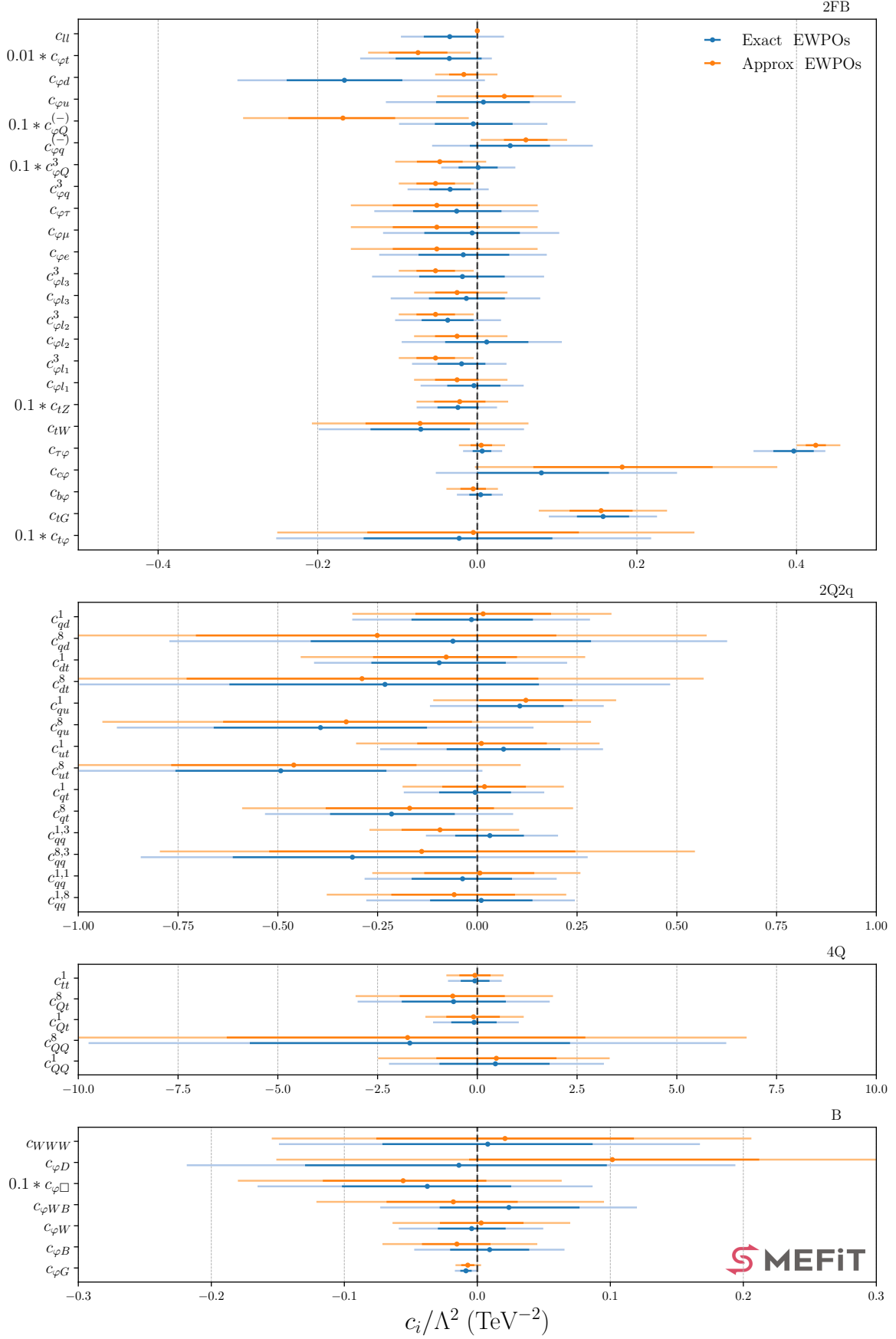



Figure A.2: The results of the global SMEFIT analysis, comparing the approximated [22, 23] and exact [39] implementation of the EWPOs. For each of the Wilson coefficients entering the fit, we indicate the best-fit results and the marginalised 68% CL (95% CL) intervals with thicker (thinner) lines. The fit labelled as “Approx EWPOs” differs slightly from that of [23] due to the use of improved theory predictions, see text for more details. Operators are grouped by type: from top to bottom, we show two-fermion-two-boson (2F2B), two-heavy-two-light (2Q2q), four-heavy quarks (4Q), and purely bosonic (B) operators.

obtained with the approximate and exact implementations. As mentioned before, the results labelled as “Approx EWPOs” differ slightly from those in [23] due to the use of improved EFT theory predictions. In general one observes good agreement between the results of the global EFT fit with approximate and exact implementation of the EWPOs, with small differences whose origin is discussed in [39].

B The MATCH2FIT package

As mentioned in the introduction, several public tools to carry out global analyses of experimental data in the SMEFT framework have been presented. Some of these tools also include the option to carry out parameter scans in the space of pre-defined UV models matched to SMEFT. While the matching procedure between UV models and the SMEFT coefficients has been automated at tree-level and partially at 1-loop level, currently there is no streamlined method enabling the interface of the output of these matching codes with SMEFT fitting frameworks. Such interface would allow using the SMEFT to impose bounds on the parameter space of general, user-defined UV-complete models.

In this appendix we describe the MATCH2FIT package used in this work to interface an EFT automated matching code, specifically MATCHMAKEREFT, with a global fitting analysis framework, in this case SMEFIT. The current public version of this package is available on [Github](#) . We emphasize that MATCH2FIT could be extended to connect different matching and fitting SMEFT codes. We provide here a succinct introduction to this code, and point the interested reader to the [user’s manual](#) for more details.

The package has two different working modes. The first one reads the matching output in the format used by MATCHMAKEREFT and parses it to the format of run cards that can be fed into SMEFIT. In this mode, the mandatory inputs are the location of the file containing the matching results and a numerical value (in TeV) for the mass of the heavy particle. Optionally, one can also specify a name for the UV model and define a “collection”, a set of UV models with common characteristics. Depending on the executed function, the code will print the run card for a scan on the UV parameters with or without the accompanying file that defines the UV invariants (see Sect. 2.3).

The second mode runs MATCHMAKEREFT to perform the tree-level matching of a certain UV model to SMEFT and generates the same final output than the previous mode. It is also possible to just perform the matching without producing the run cards for SMEFIT. The input required in this mode is the one that MATCHMAKEREFT needs to describe the heavy particles that will be integrated out. More precisely, it needs the `.fr`, `.red` and `.gauge` files, and optionally the `.red` file. The `.fr` file is just a FeynRules file that defines the heavy particle(s), its (their) free Lagrangian and its (their) interactions with the SM. The SM and SMEFT models are included in MATCHMAKEREFT and can be used in this context without further modification. See [12] for more details on how to write the `.fr` file and what the other files must contain.

The MATCH2FIT code consists of a Wolfram Mathematica Package designed and tested in version 12.1 or later. To unlock its full functionality, this package requires a working installation of MATCHMAKEREFT.

Main commands. In order to highlight its usage, we describe now the key commands made available by the MATCH2FIT package.

- `parametersList[directory,model]`: Both arguments should be strings. This function reads the file `model.fr` in `directory`, recognizes the masses and couplings of the heavy particles to be integrated out, and gives back an array with two elements. The first element is a list with the symbolical expression of the masses of the heavy particles. The second element is a list of the couplings defined for these heavy particles, excluding gauge couplings but not self-interactions.
- `parametersListFromMatchingResult[matchResFile]`: It takes as only argument a string with the address of the file containing the matching results. It recognizes the masses and couplings of the heavy particles from those results and gives an output in the same format as `parametersList`. This code

assumes that any parameter with a name starting by m or M corresponds to a mass and identifies any other parameter as a coupling. If the input of `parametersListFromMatchingResult` is the matching result obtained with the model fed into `parametersList`, any difference in their outputs should be due to couplings (or whole particles) that do not affect the tree-level matching result.

- `flavourSymChecker[matchResFile,Options]`: It takes the file with matching results specified as input and checks if those results are compatible with the SMEFIT flavour symmetry, $U(2)_q \times U(2)_u \times U(3)_d \times (U(1)_\ell \times U(1)_e)^3$. If the constraints are satisfied, it returns YES. If not, it returns NO and it prints the first WC for which it found a symmetry violation. The option "UVFlavourAssumption" allows the user to specify a replacement list that can be used to apply flavour assumptions on the UV parameters. The left-hand side of the replacement rule should contain some of the UV parameters listed by `parametersListFromMatchingResult` or `parametersList` with or without numerical indices, according to how they appear in the matching results file. The code supports up to 4 numerical indices in a single group, i.e. couplings such as g_{UV} , $g_{UV}[1]$, $g_{UV}[1,3]$ and $g_{UV}[1,3,2,4]$ are supported, but $g_{UV}[1][3]$ or $g_{UV}[1][2,3]$ are not. The default value of "UVFlavourAssumption" is an empty list. An example of how to set this option is,

```
1 {"UVFlavourAssumption" -> {gWtiQ[i_, j_] :> KroneckerDelta[i, j] * KroneckerDelta[i,
    3] gWqf[3, 3] }}
```

- `flavourSolver[matchResFile, Options]`: It takes the file with matching results specified as input and tries to solve the constraints imposed by the SMEFIT flavour symmetry, $U(2)_q \times U(2)_u \times U(3)_d \times (U(1)_\ell \times U(1)_e)^3$, for the UV couplings. The running time, the number of solutions and their complexity depend on the model. It returns all found solutions. The only Option of this function is "UVFlavourAssumption", which follows the same description given in the function `flavourSymChecker`. This function considers the SM Yukawa couplings as symbolical variables and they can be set to zero with the option "UVFlavourAssumption".
- `matcher[directory, model]`: it runs MATCHMAKEREFT and performs the tree-level matching without printing any run card for SMEFIT. It takes two strings as arguments, `directory` and `model`. The first one is the directory where the package will look for the files `model.fr`, `model.red` and `model.gauge`. If the code does not find one of those files, it will print a warning. It does not check for the existence of `model.herm`. The expected content of each of those files is specified in the documentation of MATCHMAKEREFT [12]. MATCHMAKEREFT will create the folder `directory/model_MM`, inside which the matching results will be stored as `MatchingResult.dat`. The code will check if MATCHMAKEREFT reported any problem during the matching and will print a warning if so. After performing the matching, the package will remove most of the files and directories created by itself or MATCHMAKEREFT for the sake of tidiness. It will only leave the directory `model_MM` and 2 files inside: `MatchingResult.dat` and `MatchingProblems.dat`.
- `matchResToUVscanCard[matchResFile, mass, Options]`: Function that reads the file with the tree-level matching results and prints the cards required for a UV scan. `matchResFile` must be a string with the exact address of the file that contains the matching results to be used. The format of that file should be exactly like the file `MatchingResult.dat` produced by MATCHMAKEREFT. The argument `mass` should be the value in TeV that the mass(es) of the UV particle(s) will be set to. `mass` can be one numerical value or a list of them $\{m_1, \dots, m_N\}$, the latter being useful in the case of a multiparticle model. The order of the masses is the one returned by `parametersListFromMatchingResult`. If the user specifies only one numerical mass value for a multiparticle model, all the particles will be assigned the same mass. If `parametersListFromMatchingResult` identifies K masses and $N < K$, the code will assume $m_i = m_N$ for $N \leq i \leq K$. If $N > K$, the values m_i with $K < i \leq N$ will be ignored. The mass values are also printed on the card names and inside the cards. For multiple masses, the convention is to take

the integer part of each value and stick them together in sequence. This function has 3 options. The first one is "UVFlavourAssumption", which is identical to the one of the function `flavourSymChecker`, see its description for details on this option. The second option is "Collection", a string indicating the Collection to which the model belongs. Its default value is "UserCollection". Finally, the option "Model" is a string that specifies the model name to be printed on the run cards, with default value "UserModel". An example of how to set these options is replacing the argument `Options` by:

```
1 {"UVFlavourAssumption" -> {lambdaT1[a_] :> lambdaT1[3]},
2 "Collection" -> "TestMatchingCollection", "Model"->"TestModel"}
```

The package also includes a function that integrates the steps of matching and printing all the run cards according to the result of said matching:

- `modelToUVscanCard[directory,model,mass, Options]`: Function that takes the files that define the UV model, performs the tree-level matching by running `MATCHMAKEREFT`, and prints the run cards needed for a UV scan. The first two arguments are exactly like in `matcher`, i.e. the program will look for the files `model.fr`, `model.red`, and `model.gauge` in `directory` and will do the tree-level matching based on them. The argument `model` also defines the name of the model. `mass` should be the value(s) in TeV that the mass(es) of the UV particle(s) will be set to. The handling of several mass values is equal to the function `matchResToUVscanCard`. This function has 2 options. The first one is "UVFlavourAssumption", which is identical to the one of the function `flavourSymChecker`, see its description for details on this option. The second option is "Collection", a string indicating the Collection to which the model belongs. Its default value is "UserCollection". An example of how to set these options is replacing the argument `Options` by:

```
1 {"UVFlavourAssumption" -> {lambdaT1[a_] :> lambdaT1[3]},
2 "Collection" -> "TestMatchingCollection"}
```

Limitations and outlook. In its current incarnation, all SM couplings are numerically evaluated when printing the run cards used as input in the global SMEFT fit. Their values are hard-coded in the package and summarised in App. A of the `MATCH2FIT` user manual. Future versions of `MATCH2FIT` should allow the user to vary easily these values.

Another restriction of `MATCH2FIT` is that it does not check for the fulfilment of the SMEFT flavour assumptions automatically when printing the run cards for SMEFT. This generates a degree of arbitrariness, e.g. the code uses the matching result for $(c_{\varphi q}^{(3)})_{22}$ as the result for $(c_{\varphi q}^{(3)})_{ii}$ without verifying first that $(c_{\varphi q}^{(3)})_{22} = (c_{\varphi q}^{(3)})_{11}$. We summarise these choices in App. B of the user manual. The user should be aware of this limitation and compensate for it with the required assumptions on the UV couplings. Support for alternative flavour structures on the Wilson coefficients will be added in the future, in order to ensure full compatibility with updated versions of the SMEFT analysis and/or becoming compatible with other fitting codes.

We also note that `MATCH2FIT` assumes that all UV couplings are real and applies this assumption when interpreting the matching results. The support for complex UV couplings (and hence also of the corresponding WCs) will be added in future releases.

In the long term, `MATCH2FIT` could be extended to process matching results provided in the WCxf format [50]. This would facilitate the interface with other SMEFT matching codes such as `CoDEX` and `MATCHETE` as well as with codes implementing the Renormalisation Group Equations (RGEs) running of SMEFT operators.

C Origin of the logarithms in 1-loop matching formulas.

The logarithms in one-loop matching expressions such as that of Eq. (2.11) arise as a consequence of the RG running of both the UV couplings and the EFT coefficients. Their appearance ensures that the matching

result is correct irrespective of the choice of matching scale [6, 12]. In this appendix we revisit this point in the explicit case of the heavy scalar model defined by the Lagrangian of Eq. (2.1). We start with the general expression, valid for a any matching scale Q , for the Wilson coefficient $c_{qu,pqrs}^{(8)}$, which is the most general form in flavour space of the coefficient $c_{Qt}^{(8)}$ generated by this model. Subsequently, we evaluate this matching relation at two different scales, $Q = m_\phi$ and $Q = \mu < m_\phi$, to obtain the results for $c_{qu,pqrs}^{(8)}|_{Q=m_\phi}$ and $c_{qu,pqrs}^{(8)}|_{Q=\mu}$. We expect only the former to be free of RG logarithms.

Then we use the RGEs for the Wilson coefficients in the EFT and for the UV couplings of the heavy scalar model to evolve $c_{qu,pqrs}^{(8)}|_{Q=m_\phi}$ down to the scale μ to obtain $c_{qu,pqrs}^{(8)}|_{Q=m_\phi \rightarrow \mu}$. The comparison between the two calculations, $c_{qu,pqrs}^{(8)}|_{Q=m_\phi \rightarrow \mu}$ and $c_{qu,pqrs}^{(8)}|_{Q=\mu}$, will tell us whether the logarithms arising in the general matching formula correspond to the ones generated by the RG running or not. This procedure, which was also adopted in App. C of [12], is sketched in Fig. C.1.

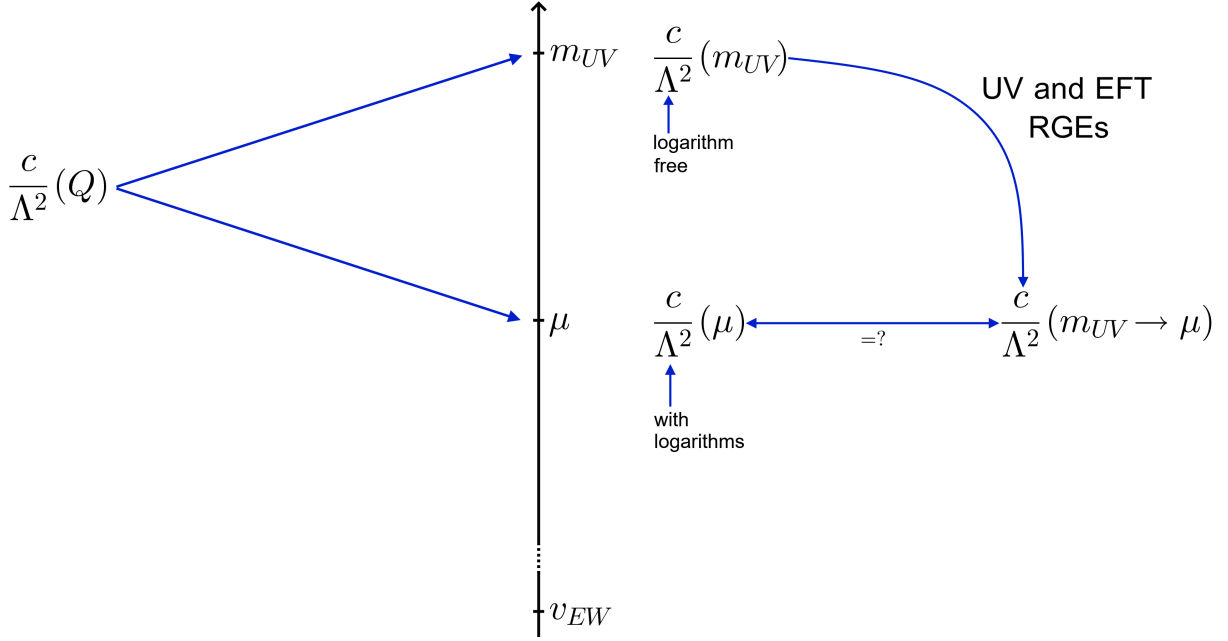


Figure C.1: Sketch of the procedure adopted to verify the origin of the logarithms arising in the one-loop matching formulas. The general matching expression for the EFT coefficient c/Λ^2 in terms of UV couplings is evaluated at two different scales, $Q = m_{UV}$ and $Q = \mu < m_{UV}$, and one verify whether or not the two results are entirely related by RGE running.

For illustration purposes, we perform this check separately at $\mathcal{O}(g_3^2)$ and then at $\mathcal{O}(g_1^2)$, i.e. the contributions that depends on the matching scale Q will only be kept at that order. On the other hand, we perform it without applying any flavour assumption on the EFT coefficient nor the UV model.

Order g_3^2 validation. The starting point of this calculation is the general matching result at one-loop for the Wilson coefficient $c_{qu,prst}^{(8)}$ in the heavy scalar model, given by

$$\begin{aligned}
\frac{c_{qu,prst}^{(8)}}{\Lambda^2} = & -\frac{(y_\phi^u)_{pt}(y_\phi^u)_{rs}^*}{m_\phi^2} - \frac{g_3^2 \delta_{s,t}(y_\phi^d)_{ir}(y_\phi^d)_{ip}^*}{144\pi^2 m_\phi^2} \left(4 - 3 \log\left(\frac{m_\phi^2}{Q^2}\right)\right) \\
& - \frac{g_3^2 \delta_{p,r}(y_\phi^u)_{it}(y_\phi^u)_{is}^*}{72\pi^2 m_\phi^2} \left(4 - 3 \log\left(\frac{m_\phi^2}{Q^2}\right)\right) - \frac{g_3^2 \delta_{s,t}(y_\phi^u)_{pi}(y_\phi^u)_{ri}^*}{144\pi^2 m_\phi^2} \left(4 - 3 \log\left(\frac{m_\phi^2}{Q^2}\right)\right) \\
& + \frac{g_3^2 (y_\phi^u)_{pt}(y_\phi^u)_{rs}^*}{48\pi^2 m_\phi^2} + \mathcal{O}\left(\frac{g_3^0}{16\pi^2}\right), \tag{C.1}
\end{aligned}$$

where $prst$ indicate the flavour indices and we omitted the one-loop contributions that do not depend on the g_3 coupling. As expected, all the logarithms appearing in this expression are removed by setting the matching scale at the heavy scalar mass, $Q = m_\phi$.

The renormalisation group equations relevant to describe the scale dependence of this specific Wilson coefficient are given by [51],

$$\begin{aligned} \mu \frac{dc_{qu,prst}^{(8)}}{d\mu} &= \frac{\beta(c_{qu,prst}^{(8)})}{16\pi^2} = \frac{g_3^2}{16\pi^2} \left(\frac{4}{3} \delta_{s,t} \left(c_{qq,pj jr}^{(1)} + c_{qq,jr pj}^{(1)} \right) + 4 \delta_{s,t} \left(c_{qq,pj jr}^{(3)} + c_{qq,jr pj}^{(3)} \right) \right. \\ &\quad + \frac{2}{3} \delta_{s,t} \left(c_{qu,pr jj}^{(8)} + c_{qd,pr jj}^{(8)} \right) + \frac{4}{3} \delta_{p,r} c_{qu,jj st}^{(8)} + \frac{2}{3} \delta_{p,r} c_{ud,st jj}^{(8)} \\ &\quad \left. + \frac{4}{3} \delta_{p,r} c_{uu,sj jt} + \frac{4}{3} \delta_{p,r} c_{uu,jt sj} - 14 c_{qu,prst}^{(8)} - 12 c_{qu,prst}^{(1)} \right), \end{aligned} \quad (\text{C.2})$$

$$\mu \frac{d(y_\phi^u)_{pt}}{d\mu} = \frac{\beta\left((y_\phi^u)_{pt}\right)}{16\pi^2} = -\frac{g_3^2}{2\pi^2} (y_\phi^u)_{pt}, \quad (\text{C.3})$$

$$\mu \frac{dm_\phi}{d\mu} = 0, \quad (\text{C.4})$$

where again we have kept only those terms proportional to g_3^2 . The RGE equations for the Yukawa coupling $(y_\phi^u)_{pt}$ and the heavy mass m_ϕ were computed with RGBETA [52] and cross-checked against the results of [53]. We can solve these RGEs at leading log accuracy to obtain,

$$c_{qu,prst}^{(8)}(\mu) = c_{qu,prst}^{(8)}(m_\phi) + \frac{\beta(c_{qu,prst}^{(8)})}{32\pi^2} \log\left(\frac{\mu^2}{m_\phi^2}\right), \quad (\text{C.5})$$

and similarly for $(y_\phi^u)_{pt}$, while m_ϕ is constant at this order. The required tree-level matching results are,

$$c_{qq,ijkl}^{(1)} = c_{qq,ijkl}^{(3)} = c_{ud,ijkl}^{(8)} = c_{uu,ijkl} = 0, \quad (\text{C.6})$$

$$\frac{c_{qd,ijkl}^{(8)}}{\Lambda^2} = -\frac{(y_\phi^d)_{kj} (y_\phi^d)_{li}^*}{m_\phi^2}, \quad (\text{C.7})$$

$$\frac{c_{qu,ijkl}^{(1)}}{\Lambda^2} = -\frac{(y_\phi^u)_{il} (y_\phi^u)_{jk}^*}{6 m_\phi^2}, \quad (\text{C.8})$$

which substituting in the corresponding beta function allows one to compute $\frac{c_{qu,prst}^{(8)}}{\Lambda^2} \Big|_{Q=\mu}$ as,

$$\begin{aligned} \frac{c_{qu,prst}^{(8)}}{\Lambda^2} \Big|_{Q=\mu} &= \frac{c_{qu,prst}^{(8)}}{\Lambda^2} \Big|_{Q=m_\phi} + \frac{\beta(c_{qu,prst}^{(8)})}{32\pi^2 \Lambda^2} \log\left(\frac{\mu^2}{m_\phi^2}\right), \\ &= \frac{c_{qu,prst}^{(8)}}{\Lambda^2} \Big|_{\text{tree}, Q=m_\phi} + \frac{c_{qu,prst}^{(8)}}{\Lambda^2} \Big|_{\text{loop}, Q=m_\phi} + \frac{\beta(c_{qu,prst}^{(8)})}{32\pi^2 \Lambda^2} \log\left(\frac{\mu^2}{m_\phi^2}\right), \end{aligned} \quad (\text{C.9})$$

where we have defined

$$\frac{c_{qu,prst}^{(8)}}{\Lambda^2} \Big|_{\text{loop}, Q=m_\phi} = -\frac{g_3^2 \delta_{s,t} (y_\phi^d)_{ir} (y_\phi^d)_{ip}^*}{36\pi^2 m_\phi^2} - \frac{g_3^2 \delta_{p,r} (y_\phi^u)_{it} (y_\phi^u)_{is}^*}{18\pi^2 m_\phi^2} - \frac{g_3^2 \delta_{s,t} (y_\phi^u)_{pi} (y_\phi^u)_{ri}^*}{36\pi^2 m_\phi^2} + \frac{g_3^2 (y_\phi^u)_{pt} (y_\phi^u)_{rs}^*}{48\pi^2 m_\phi^2}. \quad (\text{C.10})$$

The last term in Eq. (C.9) is the contribution related to the running between $Q = m_\phi$ and $Q = \mu < m_\phi$.

To keep everything consistently at leading-log and one-loop order, all the couplings in the previous expression should be considered as constant with energy, and hence $\left(c_{qu,prst}^{(8)}/\Lambda^2\right) \Big|_{\text{loop}, Q=m_\phi}$ is equal to

$\left. (c_{qu,prst}^{(8)}/\Lambda^2) \right|_{\text{loop}, Q=\mu}$ except for the logarithmic pieces. The same is not true for the tree-level contribution, which has to be transformed as follows.

$$\begin{aligned}
\left. \frac{c_{qu,prst}^{(8)}}{\Lambda^2} \right|_{\text{tree}, Q=m_\phi} &= - \frac{(y_\phi^u)_{pt} (y_\phi^u)_{rs}^*}{m_\phi^2} \Big|_{Q=m_\phi} = - \frac{(y_\phi^u(m_\phi))_{pt} (y_\phi^u(m_\phi))_{rs}^*}{m_\phi^2} \\
&= - \frac{\left((y_\phi^u(\mu))_{pt} - \frac{\beta((y_\phi^u)_{pt})}{32\pi^2} \log\left(\frac{\mu^2}{m_\phi^2}\right) \right) \left((y_\phi^u(\mu))_{rs} - \frac{\beta((y_\phi^u)_{rs})}{32\pi^2} \log\left(\frac{\mu^2}{m_\phi^2}\right) \right)^*}{m_\phi^2} \\
&= - \frac{(y_\phi^u)_{pt} (y_\phi^u)_{rs}^*}{m_\phi^2} \Big|_{Q=\mu} + \frac{\beta((y_\phi^u)_{pt}) (y_\phi^u)_{rs}^*}{32\pi^2 m_\phi^2} \log\left(\frac{\mu^2}{m_\phi^2}\right) + \frac{(y_\phi^u)_{pt} \beta((y_\phi^u)_{rs})^*}{32\pi^2 m_\phi^2} \log\left(\frac{\mu^2}{m_\phi^2}\right),
\end{aligned} \tag{C.11}$$

where in the first two lines we indicate explicitly the scale at which the UV couplings are evaluated and in the last line we have kept only the leading log terms. The first term in the last line can be identified as $\left. (c_{qu,prst}^{(8)}/\Lambda^2) \right|_{\text{tree}, Q=\mu}$. Hence, now we have,

$$\left. \frac{c_{qu,prst}^{(8)}}{\Lambda^2} \right|_{Q=\mu} = \left. \frac{c_{qu,prst}^{(8)}}{\Lambda^2} \right|_{\text{tree}, Q=\mu} + \left. \frac{c_{qu,prst}^{(8)}}{\Lambda^2} \right|_{\text{loop}, Q=m_\phi} + \frac{\beta((y_\phi^u)_{pt}) (y_\phi^u)_{rs}^* + (y_\phi^u)_{pt} \beta((y_\phi^u)_{rs})^* + \beta(c_{qu,prst}^{(8)})}{32\pi^2 m_\phi^2} \log\left(\frac{\mu^2}{m_\phi^2}\right).$$

Finally, one has to replace the expressions for the β functions computed before, use the tree-level matching results inside the β function for the Wilson coefficient, and reorder the terms. This leads to Eq. (C.2) evaluated at $Q = \mu$, concluding the check.

Order g_1^2 validation. Next we perform the same check at order g_1^2 . The general matching result at 1-loop for $c_{qu,prst}^{(8)}$ is

$$\left. \frac{c_{qu,prst}^{(8)}}{\Lambda^2} \right|_{Q=\mu} = - \frac{(y_\phi^u)_{pt} (y_\phi^u)_{rs}^*}{m_\phi^2} - \frac{25g_1^2 (y_\phi^u)_{pt} (y_\phi^u)_{rs}^*}{1152\pi^2 m_\phi^2} + \mathcal{O}\left(\frac{g_1^0}{16\pi^2}\right), \tag{C.12}$$

where the omitted terms are 1-loop contributions that do not depend on g_1 . In this case, there are no logarithms in the expression. Hence, the only terms that have a dependence on the energy scale are the ones generated at tree level.

The RGE equations we need are in this case are [51, 53],

$$\mu \frac{dc_{qu,prst}^{(8)}}{d\mu} = \frac{\beta(c_{qu,prst}^{(8)})}{16\pi^2} = - \frac{g_1^2}{12\pi^2} c_{qu,prst}^{(8)}, \tag{C.13}$$

$$\mu \frac{d(y_\phi^u)_{pt}}{d\mu} = \frac{\beta((y_\phi^u)_{pt})}{16\pi^2} = - \frac{17g_1^2}{192\pi^2} (y_\phi^u)_{pt}, \tag{C.14}$$

$$\mu \frac{dm_\phi}{d\mu} = \frac{\beta(m_\phi)}{16\pi^2} = - \frac{3g_1^2}{64\pi^2} m_\phi, \tag{C.15}$$

where we have kept only those terms proportional to g_1^2 . The leading-log solution reads,

$$c_{qu,prst}^{(8)}(\mu) = c_{qu,prst}^{(8)}(m_\phi) + \frac{\beta(c_{qu,prst}^{(8)})}{32\pi^2} \log\left(\frac{\mu^2}{m_\phi^2}\right), \tag{C.16}$$

$$m_\phi^2(m_\phi) = m_\phi^2(\mu) - m_\phi(\mu) \frac{\beta(m_\phi)}{16\pi^2} \log\left(\frac{\mu^2}{m_\phi^2}\right), \tag{C.17}$$

and analogously for the UV coupling.

All the required tree-level matching results were shown in the previous subsection. We can compute

$$\begin{aligned} \frac{c_{qu,prst}^{(8)}}{\Lambda^2} \Big|_{Q=\mu} & \text{ as,} \\ \frac{c_{qu,prst}^{(8)}}{\Lambda^2} \Big|_{Q=\mu} & = \frac{c_{qu,prst}^{(8)}}{\Lambda^2} \Big|_{Q=m_\phi} + \frac{\beta(c_{qu,prst}^{(8)})}{32\pi^2\Lambda^2} \log\left(\frac{\mu^2}{m_\phi^2}\right), \\ & = \frac{c_{qu,prst}^{(8)}}{\Lambda^2} \Big|_{\text{tree},Q=m_\phi} + \frac{c_{qu,prst}^{(8)}}{\Lambda^2} \Big|_{\text{loop},Q=m_\phi} + \frac{\beta(c_{qu,prst}^{(8)})}{32\pi^2\Lambda^2} \log\left(\frac{\mu^2}{m_\phi^2}\right), \end{aligned} \quad (\text{C.18})$$

where

$$\frac{c_{qu,prst}^{(8)}}{\Lambda^2} \Big|_{\text{loop},Q=m_\phi} = -\frac{25g_1^2(y_\phi^u)_{pt}(y_\phi^u)_{rs}^*}{1152\pi^2 m_\phi^2}. \quad (\text{C.19})$$

Let us remark again that all the UV couplings in $\frac{c_{qu,prst}^{(8)}}{\Lambda^2} \Big|_{\text{loop},Q=m_\phi}$ should be considered as constant with energy. The tree-level contribution at the two different scales are related as,

$$\begin{aligned} \frac{c_{qu,prst}^{(8)}}{\Lambda^2} \Big|_{\text{tree},Q=m_\phi} & = -\frac{(y_\phi^u)_{pt}(y_\phi^u)_{rs}^*}{m_\phi^2} \Big|_{Q=m_\phi} = -\frac{(y_\phi^u(m_\phi))_{pt}(y_\phi^u(m_\phi))_{rs}^*}{m_\phi^2} \\ & = -\frac{\left((y_\phi^u(\mu))_{pt} - \frac{\beta((y_\phi^u)_{pt})}{32\pi^2} \log\left(\frac{\mu^2}{m_\phi^2}\right) \right) \left((y_\phi^u(\mu))_{rs} - \frac{\beta((y_\phi^u)_{rs})}{32\pi^2} \log\left(\frac{\mu^2}{m_\phi^2}\right) \right)^*}{m_\phi^2(\mu) - m_\phi(\mu) \frac{\beta(m_\phi)}{16\pi^2} \log\left(\frac{\mu^2}{m_\phi^2}\right)} \\ & = -\frac{(y_\phi^u)_{pt}(y_\phi^u)_{rs}^*}{m_\phi^2} \Big|_{Q=\mu} + \frac{\beta((y_\phi^u)_{pt})(y_\phi^u)_{rs}^* + (y_\phi^u)_{pt}\beta((y_\phi^u)_{rs})^*}{32\pi^2 m_\phi^2} \log\left(\frac{\mu^2}{m_\phi^2}\right) \\ & \quad - \frac{(y_\phi^u)_{pt}(y_\phi^u)_{rs}^*}{m_\phi^2} \frac{\beta(m_\phi)}{16\pi^2 m_\phi} \log\left(\frac{\mu^2}{m_\phi^2}\right), \end{aligned} \quad (\text{C.20})$$

where we have kept only the leading-log terms. The first term in the last line is $\frac{c_{qu,prst}^{(8)}}{\Lambda^2} \Big|_{\text{tree},Q=\mu}$.

Hence, in total we have,

$$\begin{aligned} \frac{c_{qu,prst}^{(8)}}{\Lambda^2} \Big|_{Q=\mu} & = \frac{c_{qu,prst}^{(8)}}{\Lambda^2} \Big|_{\text{tree},Q=\mu} + \frac{c_{qu,prst}^{(8)}}{\Lambda^2} \Big|_{\text{loop},Q=m_\phi} \\ & \quad + \frac{\beta((y_\phi^u)_{pt})(y_\phi^u)_{rs}^* + (y_\phi^u)_{pt}\beta((y_\phi^u)_{rs})^* - 2\frac{\beta(m_\phi)}{m_\phi}(y_\phi^u)_{pt}(y_\phi^u)_{rs}^* + \frac{m_\phi^2}{\Lambda^2}\beta(c_{qu,prst}^{(8)})}{32\pi^2 m_\phi^2} \log\left(\frac{\mu^2}{m_\phi^2}\right). \end{aligned}$$

Replacing the β functions computed before and reordering, one finds that the logarithmic term vanishes exactly, in perfect agreement with Eq. (C.12).

Finally, let us remark the key role played by the RGEs of the UV variables, y_ϕ^u and m_ϕ , in both checks at order g_2^2 and g_1^2 . Had we not considered them, there would have been residual logarithmic effects not accounted for by the RGEs, as found in [17]. The same checks can be performed with other WCs and at all orders in the couplings.

D Additional details on UV models.

In this appendix we provide complementary information on the UV-complete scenarios studied in this work, in particular concerning the tree-level matched one-particle models.

Scalars		Fermions		Vectors	
Model	UV couplings	Model	UV couplings	Model	UV couplings
\mathcal{S}	$\kappa_{\mathcal{S}}$	N	$(\lambda_N^e)_3$	\mathcal{B}	$(g_B^u)_{33}, (g_B^q)_{33}, g_B^\varphi,$
ϕ	$\lambda_\phi, (y_\phi^u)_{33}$	E	$(\lambda_E)_3$		$(g_B^e)_{11}, (g_B^e)_{22}, (g_B^e)_{33},$
Ξ	κ_Ξ	Δ_1	$(\lambda_{\Delta_1})_3$		$(g_B^l)_{22}, (g_B^l)_{33}$
Ξ_1	κ_{Ξ_1}	Δ_3	$(\lambda_{\Delta_3})_3$	\mathcal{B}_1	$g_{\mathcal{B}_1}^\varphi$
ω_1	$(y_{\omega_1}^{qq})_{33}$	Σ	$(\lambda_\Sigma)_3$	\mathcal{W}	$(g_{\mathcal{W}}^l)_{11} = 2 (g_{\mathcal{W}}^l)_{22}, (g_{\mathcal{W}}^l)_{33}$
ω_4	$(y_{\omega_4}^{uu})_{33}$	Σ_1	$(\lambda_{\Sigma_1})_3$		$g_{\mathcal{W}}^\varphi, (g_{\mathcal{W}}^q)_{33}$
ζ	$(y_\zeta^{qq})_{33}$	U	$(\lambda_U)_3$	\mathcal{W}_1	$g_{\mathcal{W}_1}^\varphi$
Ω_1	$(y_{\Omega_1}^{qq})_{33}$	D	$(\lambda_D)_3$	\mathcal{G}	$(g_{\mathcal{G}}^q)_{33}, (g_{\mathcal{G}}^u)_{33}$
Ω_4	$(y_{\Omega_4})_{33}$	Q_1	$(\lambda_{Q_1}^u)_3$		
Υ	$(y_\Upsilon)_{33}$	Q_7	$(\lambda_{Q_7})_3$	\mathcal{H}	$(g_{\mathcal{H}})_{33}$
Φ	$(y_\Phi^{qu})_{33}$	T_1	$(\lambda_{T_1})_3$	\mathcal{Q}_5	$(g_{\mathcal{Q}_5}^{uq})_{33}$
		T_2	$(\lambda_{T_2})_3$	\mathcal{Y}_5	$(g_{\mathcal{Y}_5})_{33}$

Table D.1: For each of the one-particle UV models considered in this work and described in Table 4.1, we list the couplings entering their Lagrangian, restricting ourselves to those which are consistent with the SMEF_{IT} flavour assumption after tree-level matching.

For each of the one-particle UV models considered here and listed in Table 4.1, we indicate the relevant couplings entering their Lagrangian in Table D.1, where as elsewhere in the paper we follow the notation from [3]. These are the UV parameters which are constrained from the data via the matching procedure. These couplings have been selected such that the resulting Wilson coefficients at the matching scale fulfil the SMEF_{IT} flavour assumptions in the case of tree-level matching.

It is worth noting that in most models considered, the interaction with the top quark is singled out and treated differently from the lighter quarks, consistently with the SMEF_{IT} assumptions. This is a well-motivated assumption and is realised in many common UV scenarios, such as in partial compositeness. Concerning the leptonic sector, the SMEF_{IT} flavour assumption allows for independent couplings to the different generations.

This situation differs from the models considered by the FITMAKER collaboration [16], in which the same heavy particles are used but the couplings are assumed to be flavour-universal. For the case of heavy spin-one bosons, they assume couplings only to the Higgs boson where appropriate. The FITMAKER models BB_1 and Q_{17} arise by considering the pairs of heavy particles $\{\mathcal{B}, \mathcal{B}_1\}$ and $\{Q_1, Q_7\}$ respectively, with degenerate masses and couplings. The models T and TB contain the heavy fermions U and Q_1 respectively with specially rescaled couplings [54].

Table D.2 indicates, for the UV models considered in the FITMAKER study [16] and which are compared with our results in Fig. 4.6, whether they comply with the flavour symmetry assumed in SMEF_{IT}, and if this is not the case what are the differences. Here “more restrictive than SMEF_{IT}” means that applying the SMEF_{IT} flavour symmetry induces more non-vanishing UV couplings than in the FITMAKER case. For the purposes of the benchmark comparison of Fig. 4.6, the effect of these additional symmetry-breaking

Wilson coefficients has been ignored.

Model	Compliant	Details
$\mathcal{S}(S)$	Yes	-
ϕ	No	$(c_{ledq})_{3333} \neq 0, (c_{quqd})_{3333} \neq 0, (c_{lequ})_{3333} \neq 0$
Ξ	Yes	-
Ξ_1	Yes	-
$\mathcal{B}(B)$	Yes	More restrictive than SMEF _{IT}
$\mathcal{B}_1(B_1)$	Yes	-
$\mathcal{W}(W)$	Yes	More restrictive than SMEF _{IT}
$\mathcal{W}_1(W_1)$	Yes	More restrictive than SMEF _{IT}
N	No	$(c_{\varphi l}^{(1),(3)})_{ij} \neq 0$ for $i \neq j$
E	No	$(c_{\varphi l}^{(1),(3)})_{ij} \neq 0$ for $i \neq j$
T	Yes	-
Δ_1	No	$(c_{\varphi e})_{ij} \neq 0$ for $i \neq j$
Δ_3	No	$(c_{\varphi e})_{ij} \neq 0$ for $i \neq j$
Σ	No	$(c_{\varphi l}^{(1),(3)})_{ij} \neq 0$ for $i \neq j$
Σ_1	No	$(c_{\varphi l}^{(1),(3)})_{ij} \neq 0$ for $i \neq j$
U	No	$(c_{\varphi q}^{(1),(3)})_{ij} \neq 0$ and $(c_{u\varphi})_{ij} \neq 0$ for $i \neq j$
D	No	$(c_{\varphi q}^{(1),(3)})_{ij} \neq 0$ for $i \neq j$
Q_5	No	$(c_{\varphi d})_{ij} \neq 0$ for $i \neq j$
Q_7	No	$(c_{\varphi u, u\varphi})_{ij} \neq 0$ for $i \neq j$
T_1	No	$(c_{\varphi q}^{(1),(3)})_{ij} \neq 0$ and $(c_{u\varphi})_{ij} \neq 0$ for $i \neq j$
T_2	No	$(c_{\varphi q}^{(1),(3)})_{ij} \neq 0$ and $(c_{u\varphi})_{ij} \neq 0$ for $i \neq j$
$U(T)$	Yes	-
$Q_1(TB)$	No	$(c_{\varphi d})_{33} \neq (c_{\varphi d})_{11,22}$ and $(c_{\varphi ud})_{33} \neq 0$
$Q_{17}(\{Q_1, Q_7\})$	Yes	-
$BB_1(\{B, B_1\})$	Yes	-

Table D.2: For the UV models considered in the FITMAKER study and which are compared with the results of our analysis in Fig. 4.6, we indicate whether they comply with the flavour symmetry assumed in SMEF_{IT}, and if this is not the case what are the differences. Here “more restrictive than SMEF_{IT}” means that applying the SMEF_{IT} flavour symmetry induces more non-vanishing UV couplings. We denote UV models following the notation of [3] and we indicate the choice in FITMAKER between parenthesis whenever different. The only model for which we use a different notation from [3] is the scalar doublet model ϕ .

References

- [1] G. Isidori, F. Wilsch and D. Wyler, *The Standard Model effective field theory at work*, [2303.16922](#).
- [2] J. Fuentes-Martin, J. Portoles and P. Ruiz-Femenia, *Integrating out heavy particles with functional methods: a simplified framework*, *JHEP* **09** (2016) 156 [[1607.02142](#)].
- [3] J. de Blas, J. C. Criado, M. Perez-Victoria and J. Santiago, *Effective description of general extensions of the Standard Model: the complete tree-level dictionary*, *JHEP* **03** (2018) 109 [[1711.10391](#)].
- [4] S. Das Bakshi, J. Chakraborty and S. K. Patra, *CoDEx: Wilson coefficient calculator connecting SMEFT to UV theory*, *Eur. Phys. J. C* **79** (2019) 21 [[1808.04403](#)].
- [5] M. Krämer, B. Summ and A. Voigt, *Completing the scalar and fermionic Universal One-Loop Effective Action*, *JHEP* **01** (2020) 079 [[1908.04798](#)].
- [6] V. Gherardi, D. Marzocca and E. Venturini, *Matching scalar leptiquarks to the SMEFT at one loop*, *JHEP* **07** (2020) 225 [[2003.12525](#)].
- [7] A. Angelescu and P. Huang, *Integrating Out New Fermions at One Loop*, *JHEP* **01** (2021) 049 [[2006.16532](#)].
- [8] S. A. R. Ellis, J. Quevillon, P. N. H. Vuong, T. You and Z. Zhang, *The Fermionic Universal One-Loop Effective Action*, *JHEP* **11** (2020) 078 [[2006.16260](#)].
- [9] T. Cohen, X. Lu and Z. Zhang, *STrEAMlining EFT Matching*, *SciPost Phys.* **10** (2021) 098 [[2012.07851](#)].
- [10] J. Fuentes-Martin, M. König, J. Pagès, A. E. Thomsen and F. Wilsch, *SuperTracer: A Calculator of Functional Supertraces for One-Loop EFT Matching*, *JHEP* **04** (2021) 281 [[2012.08506](#)].
- [11] B. Summ, *One Formula To Match Them All: The Bispinor Universal One-Loop Effective Action*, Ph.D. thesis, RWTH Aachen U., 2020. [2103.02487](#). 10.18154/RWTH-2021-00828.
- [12] A. Carmona, A. Lazopoulos, P. Olgoso and J. Santiago, *Matchmakereft: automated tree-level and one-loop matching*, *SciPost Phys.* **12** (2022) 198 [[2112.10787](#)].
- [13] J. Fuentes-Martín, M. König, J. Pagès, A. E. Thomsen and F. Wilsch, *Evanescence operators in one-loop matching computations*, *JHEP* **02** (2023) 031 [[2211.09144](#)].
- [14] J. Fuentes-Martín, M. König, J. Pagès, A. E. Thomsen and F. Wilsch, *A proof of concept for matchete: an automated tool for matching effective theories*, *Eur. Phys. J. C* **83** (2023) 662 [[2212.04510](#)].
- [15] S. De Angelis and G. Durieux, *EFT matching from analyticity and unitarity*, [2308.00035](#).
- [16] J. Ellis, M. Madigan, K. Mimasu, V. Sanz and T. You, *Top, Higgs, Diboson and Electroweak Fit to the Standard Model Effective Field Theory*, *JHEP* **04** (2021) 279 [[2012.02779](#)].
- [17] I. Brivio, S. Bruggisser, E. Geoffray, W. Kilian, M. Krämer, M. Luchmann et al., *From Models to SMEFT and Back?*, *SciPost Phys.* **12** (2022) 036 [[2108.01094](#)].
- [18] Anisha, S. Das Bakshi, S. Banerjee, A. Biekötter, J. Chakraborty, S. Kumar Patra et al., *Effective limits on single scalar extensions in the light of recent LHC data*, *Phys. Rev. D* **107** (2023) 055028 [[2111.05876](#)].
- [19] N. P. Hartland, F. Maltoni, E. R. Nocera, J. Rojo, E. Slade, E. Vryonidou et al., *A Monte Carlo global analysis of the Standard Model Effective Field Theory: the top quark sector*, *JHEP* **04** (2019) 100 [[1901.05965](#)].
- [20] S. van Beek, E. R. Nocera, J. Rojo and E. Slade, *Constraining the SMEFT with Bayesian reweighting*, *SciPost Phys.* **7** (2019) 070 [[1906.05296](#)].
- [21] J. J. Ethier, R. Gomez-Ambrosio, G. Magni and J. Rojo, *SMEFT analysis of vector boson scattering and diboson data from the LHC Run II*, *Eur. Phys. J. C* **81** (2021) 560 [[2101.03180](#)].
- [22] SMEFT collaboration, *Combined SMEFT interpretation of Higgs, diboson, and top quark data from the LHC*, *JHEP* **11** (2021) 089 [[2105.00006](#)].
- [23] T. Giani, G. Magni and J. Rojo, *SMEFT: a flexible toolbox for global interpretations of particle physics data with effective field theories*, *Eur. Phys. J. C* **83** (2023) 393 [[2302.06660](#)].
- [24] I. Brivio and M. Trott, *The Standard Model as an Effective Field Theory*, *Phys. Rept.* **793** (2019) 1 [[1706.08945](#)].

- [25] S. A. R. Ellis, J. Quevillon, T. You and Z. Zhang, *Extending the Universal One-Loop Effective Action: Heavy-Light Coefficients*, *JHEP* **08** (2017) 054 [[1706.07765](#)].
- [26] J. F. Gunion and H. E. Haber, *The CP conserving two Higgs doublet model: The Approach to the decoupling limit*, *Phys. Rev. D* **67** (2003) 075019 [[hep-ph/0207010](#)].
- [27] J. Bernon, J. F. Gunion, H. E. Haber, Y. Jiang and S. Kraml, *Scrutinizing the alignment limit in two-Higgs-doublet models: $m_h=125$ GeV*, *Phys. Rev. D* **92** (2015) 075004 [[1507.00933](#)].
- [28] J. C. Criado, *MatchingTools: a Python library for symbolic effective field theory calculations*, *Comput. Phys. Commun.* **227** (2018) 42 [[1710.06445](#)].
- [29] B. Grzadkowski, M. Iskrzynski, M. Misiak and J. Rosiek, *Dimension-Six Terms in the Standard Model Lagrangian*, *JHEP* **10** (2010) 085 [[1008.4884](#)].
- [30] M. Chala, A. Díaz-Carmona and G. Guedes, *A Green's basis for the bosonic SMEFT to dimension 8*, *JHEP* **05** (2022) 138 [[2112.12724](#)].
- [31] Z. Ren and J.-H. Yu, *A Complete Set of the Dimension-8 Green's Basis Operators in the Standard Model Effective Field Theory*, [2211.01420](#).
- [32] R. Aoude, F. Maltoni, O. Mattelaer, C. Severi and E. Vryonidou, *Renormalisation group effects on SMEFT interpretations of LHC data*, [2212.05067](#).
- [33] PARTICLE DATA GROUP collaboration, *Review of Particle Physics*, *PTEP* **2022** (2022) 083C01.
- [34] C. Zhang, *SMEFTs living on the edge: determining the UV theories from positivity and extremality*, *JHEP* **12** (2022) 096 [[2112.11665](#)].
- [35] ALEPH, DELPHI, L3, OPAL, SLD, LEP ELECTROWEAK WORKING GROUP, SLD ELECTROWEAK GROUP, SLD HEAVY FLAVOUR GROUP collaboration, *Precision electroweak measurements on the Z resonance*, *Phys. Rept.* **427** (2006) 257 [[hep-ex/0509008](#)].
- [36] ATLAS collaboration, *Combined effective field theory interpretation of Higgs boson and weak boson production and decay with ATLAS data and electroweak precision observables*, tech. rep., CERN, Geneva, 2022.
- [37] J. Alwall, R. Frederix, S. Frixione, V. Hirschi, F. Maltoni, O. Mattelaer et al., *The automated computation of tree-level and next-to-leading order differential cross sections, and their matching to parton shower simulations*, *JHEP* **07** (2014) 079 [[1405.0301](#)].
- [38] C. Degrande, G. Durieux, F. Maltoni, K. Mimasu, E. Vryonidou and C. Zhang, *Automated one-loop computations in the standard model effective field theory*, *Phys. Rev. D* **103** (2021) 096024 [[2008.11743](#)].
- [39] SMEFT collaboration, *Electroweak precision observables in the SMEFT from LEP to future colliders, in preparation* (2023) .
- [40] D. Marzocca et al., *BSM Benchmarks for Effective Field Theories in Higgs and Electroweak Physics*, [2009.01249](#).
- [41] G. E. Box and G. C. Tiao, *Standard Normal Theory Inference Problems*, ch. 2, pp. 76–148. John Wiley and Sons, Ltd. <https://doi.org/10.1002/9781118033197>.
- [42] L. Di Luzio, J. F. Kamenik and M. Nardecchia, *Implications of perturbative unitarity for scalar di-boson resonance searches at LHC*, *Eur. Phys. J. C* **77** (2017) 30 [[1604.05746](#)].
- [43] D. Barducci, M. Nardecchia and C. Toni, *Perturbative unitarity constraints on generic vector interactions*, [2306.11533](#).
- [44] F. Feroz, M. P. Hobson, E. Cameron and A. N. Pettitt, *Importance Nested Sampling and the MultiNest Algorithm*, *Open J. Astrophys.* **2** (2019) 10 [[1306.2144](#)].
- [45] F. Feroz and M. P. Hobson, *Multimodal nested sampling: an efficient and robust alternative to MCMC methods for astronomical data analysis*, *Mon. Not. Roy. Astron. Soc.* **384** (2008) 449 [[0704.3704](#)].
- [46] I. Brivio and M. Trott, *Scheming in the SMEFT... and a reparameterization invariance!*, *JHEP* **07** (2017) 148 [[1701.06424](#)].
- [47] Z. Kassabov, M. Madigan, L. Mantani, J. Moore, M. Morales Alvarado, J. Rojo et al., *The top quark legacy of the LHC Run II for PDF and SMEFT analyses*, *JHEP* **05** (2023) 205 [[2303.06159](#)].

- [48] A. Greljo, S. Iranipour, Z. Kassabov, M. Madigan, J. Moore, J. Rojo et al., *Parton distributions in the SMEFT from high-energy Drell-Yan tails*, *JHEP* **07** (2021) 122 [[2104.02723](#)].
- [49] NNPDF collaboration, *The path to proton structure at 1% accuracy*, *Eur. Phys. J. C* **82** (2022) 428 [[2109.02653](#)].
- [50] J. Aebischer et al., *WCxf: an exchange format for Wilson coefficients beyond the Standard Model*, *Comput. Phys. Commun.* **232** (2018) 71 [[1712.05298](#)].
- [51] R. Alonso, E. E. Jenkins, A. V. Manohar and M. Trott, *Renormalization Group Evolution of the Standard Model Dimension Six Operators III: Gauge Coupling Dependence and Phenomenology*, *JHEP* **04** (2014) 159 [[1312.2014](#)].
- [52] A. E. Thomsen, *Introducing RGBeta: a Mathematica package for the evaluation of renormalization group β -functions*, *Eur. Phys. J. C* **81** (2021) 408 [[2101.08265](#)].
- [53] P. Ferreira, H. E. Haber and E. Santos, *Preserving the validity of the Two-Higgs Doublet Model up to the Planck scale*, *Phys. Rev. D* **92** (2015) 033003 [[1505.04001](#)].
- [54] S. Dawson, S. Homiller and S. D. Lane, *Putting standard model EFT fits to work*, *Phys. Rev. D* **102** (2020) 055012 [[2007.01296](#)].